Author version of the manuscript published for Canadian Journal of Forest Research on the web 30 July 2018. DOI: 10.1139/cjfr-2018-0006.
http://www.nrcresearchpress.com/toc/cjfr/0/ja

Model-based local thresholding for canopy hemispherical photography

Gastón Mauro Díaz[1, 3] and José Daniel Lencinas[1, 2]

1. Consejo Nacional de Investigaciones Científicas y Técnicas (CONICET) and the Centro de Investigación y Extensión Forestal Andino Patagónico (CIEFAP), Ruta 259 km 16,24, Esquel, Chubut, Argentina
2. Universidad Nacional de la Patagonia San Juan Bosco.
3. Corresponding author: gdiaz@correociefap.org.ar

Author version of the manuscript published for Canadian Journal of Forest Research on the web 30 July 2018. DOI: 10.1139/cjfr-2018-0006.
http://www.nrcresearchpress.com/toc/cjfr/0/ja

Abstract

Canopy hemispherical photography (HP) is widely used to estimate forest structural variables. To achieve good results with HP, a classification algorithm is needed to produce binary images to accurately estimate the gap fraction. We aimed to develop a local thresholding method for binarizing carefully acquired hemispherical photographs. The method was implemented in the R package “caiman”. Working with photographs of artificial structures and using a linear model, our method turns the cumbersome problem of finding the optimal threshold value into a simpler one, which is estimating the digital number (DN) of the sky. Using hemispherical photographs of a deciduous forest, we compared our method with several standard and state-of-the-art binarization techniques. Our method was as accurate as the best-tested binarization techniques, regardless of the exposure, as long as it was between 0 and 2 stops over the open sky auto-exposure. Moreover, our method did not require knowing the exact relative exposure. Intending to balance accuracy and practicality, we mapped the sky DN using the values extracted from gaps. However, we discussed whether a more accurate but less practical way to map sky DN could provide, along with our method, a new benchmark.

Key words: Clumping index, Exposure, Gap fraction, Leaf area index, Local thresholding

Introduction

Sustainable forest management requires information at the landscape scale and remote sensing is key for generating it (Masek et al. 2015). The validation of remote sensing products is difficult because it requires highly efficient methods to acquire the needed data (Schleppi et al. 2011). Canopy hemispherical photography (HP) is a useful method for forest variable estimation. However, it has high uncertainty in the estimation of gap fraction (GF). HP directly measures GF with high angular resolution and indirectly measures other variables, such as leaf area index (LAI) (Jonckheere et al. 2004).

Author version of the manuscript published for Canadian Journal of Forest Research on the web 30 July 2018. DOI: 10.1139/cjfr-2018-0006.
http://www.nrcresearchpress.com/toc/cjfr/0/ja

Uncertainty in HP-derived measurements is due to the lack of methods to obtain an accurate estimation of GF with high angular resolution (Jonckheere et al. 2005). The lack of methods could be solved using photographs of artificial structures with a known GF (Thimonier et al. 2010, Macfarlane et al. 2014, Song et al. 2014), but this approach has marginal usefulness for the assessment of robust image processing methods, as the one of Díaz and Lencinas (2015), because in such artificial structures the multiscattering is significantly different than in real canopies. Additionally, the effect of direct sunlight is different. On the other hand, this needed reference data could be provided by the recent groundbreaking technology of terrestrial laser scanning (Newnham et al. 2015); nevertheless, more research is needed to validate this new approach. The data obtained from radiometers (as LAI-2000 PCA, LI-COR) could be used as a benchmark, but not as a reference, because these sensors measure light, and therefore they overestimate GF because canopy elements are not optically black (Cescatti 2007). These sensors also have a low angular resolution and a high resolution is required. Therefore, the best benchmark should be carefully acquired and processed photographs.

The easiest way to estimate GF with a hemispherical photograph is to process it to obtain a binary image that represents the sky with value 1 (Sky class) and the plants with value 0 (Plant class). The easiest technique to binarize a photograph is to select a color channel and apply a global threshold value to it. Using global thresholding and the blue channel is the common practice in HP, the blue channel is used because it usually produces greatest contrast between plants and sky (Jonckheere et al. 2005). The photographs must be taken with diffuse light (Lang et al. 2010). For 8-bit images, the blue channel should have all the range of digital number (DN), from 0 to 255. In this image processing context, a bimodal histogram is the best possible scenario for HP, where the histogram peaks represent the Plant and Sky classes.

Camera exposure plays an important role in getting a good bimodal histogram because the scene luminance range is several times greater than the dynamic range of camera sensors (Beckschäfer et al. 2013). To control which segment of the scene

luminance range will be registered in the photograph, the camera user must vary both the exposure and the sensitivity of the digital system, where the former is the amount of light that reaches the sensor and the latter is the relative amount of light needed to produce an image with a defined quality (Allen and Triantaphillidou 2010, Nikon 2018). The exposure value (EV) that cameras automatically determine (auto-EV) is that which produces an image that, overall, is perceived as having a brightness similar to a middle grey (Allen and Triantaphillidou 2010). Hemispherical photographs taken with an auto-EV determined under the canopy cannot be accurately classified (Beckschäfer et al. 2013) even with high performance image processing techniques (Díaz and Lencinas 2015), being open canopies an exception. In such cases, the auto-EV tends to take into account the sky luminance, producing a bimodal histogram. Several techniques have been proposed to find the optimal exposure in HP. In photography in general, the relative EV (REV) is widely used. In HP, there are several methods to calculate the REV. The main difference between these methods is whether the EV is relative to the auto-EV for the open sky or the auto-EV under the canopy. The last approach is the simplest to do (Beckschäfer et al. 2013), but the first allows the use of REV as an accurate contrast descriptor (Zhang et al. 2005). A common practice is overexposing the sky with 2 stops of REV to open sky auto-EV (Zhang et al. 2005).

In a good bimodal histogram dark, grey and light pixels can be classified (Macfarlane 2011). Dark pixels are labeled as Plant and light pixels as Sky. Grey pixels are considered as a mixture of the dark of plants and the light of the sky. The main conclusion of Macfarlane (2011) was that the method used to classify mixed pixels in canopy images does not affect the accuracy of GF extraction once homogeneous regions of sky and canopy have been identified. The problem is that not all grey pixels are always mixed pixels, even in photographs taken with diffuse light. A given grey pixel could represent a relatively lighter plant tissue (Leblanc et al. 2005) or a relatively darker portion of the sky (Lang et al. 2010). The overcast sky is bright near the zenith and dark near the horizon, and the opposite is true for clear skies with low solar elevation (Lang et

al. 2010). Another effect that could darken a pure sky pixel is the vignetting effect. This effect obscures the borders of the images and it depends on the type and design of lens and the mechanical construction of the lens barrels (Allen and Triantaphillidou 2010). All global thresholding methods have the same drawback: ignoring the sky brightness heterogeneity and the vignetting effect (Wagner 2001).

Although global thresholding is the most widely used, there are several alternatives for obtaining binary images. Automatic thresholding algorithms can be classified as global, regional, or local. Global algorithms need to find one optimal threshold value (OTV) and regional algorithms need to find as many OTVs as regions delimited in the image, which usually are the so-called rings. In contrast, local thresholding algorithms use a moving window to find an OTV by pixel. Automatic thresholding algorithms use the content of the image to estimate the OTV. Nevertheless, using the content of the image is not the only available approach to find an OTV, as Song et al. (2014) showed. These authors published a method (the exposure-corresponding or EC) that solves the uncertainty in the determination of the OTV by relating it with the REV to open sky auto-EV (REV2OS). The EC method was calibrated by taking photographs of artificial black structures, which were developed by the authors. The photographs were taken in controlled diffuse light conditions using a lens with a long focal length to reduce the vignetting effect. Using these carefully acquired photographs of artificial structures with a known GF, Song et al. (2014) adjusted a function to predict OTV with REV2OS. Nevertheless, the EC method is a global thresholding method and thus it ignores the sky brightness heterogeneity and the vignetting effect.

Cescatti (2007) developed a method that considers the sky brightness heterogeneity and the vignetting effect. His method is grounded in physics and electronics instead of image processing. A drawback of this method is the uncertainty of using a consumer-oriented camera as a piece of radiation measuring equipment because the processes inside a camera are complex, difficult to model, and protected by trade secrets (Lang et al. 2010). In addition, this method measures the light and thus the GF is overestimated

Author version of the manuscript published for Canadian Journal of Forest Research on the web 30 July 2018. DOI: 10.1139/cjfr-2018-0006.
http://www.nrcresearchpress.com/toc/cjfr/0/ja

because canopy elements are not optically black (Cescatti 2007). Besides, the use of regional thresholding to handle sky heterogeneity was proposed but not tested (Leblanc et al. 2005). On the other hand, Wagner (1998) proposed a method for digitized film photographs. This method uses the initial value, which is the boundary between the DN of a pure sky pixel and a mixed pixel and is always higher than the OTV. The importance of the initial value is that it is linked to the pure sky DN, allowing the use of local or regional thresholding if the pure sky DN is known for each pixel by any method; however, the relationship between the initial value and the OTV remains unclear (Wagner 2001).

We saw potential in the combination of the technical approaches of Wagner (1998) and Song et al. (2014). Empirical models fitted with the data generated with canopy models, as the one used by Song et al. (2014), could overcome the disadvantage of using a consumer-oriented camera for precision measurements. On the other hand, a local thresholding method based on knowing the sky brightness for every pixel of the image, as Wagner (1998) proposed, could overcome the drawbacks of global thresholding.

Our goal was to contribute to the development of methods for obtaining accurate estimations of GF with high angular resolution. Our objective was to develop a model-based local thresholding method to binarize carefully acquired canopy hemispherical photographs. To this end, we used hemispherical photographs of a deciduous forest and pictures of the open sky. We compared our method against both standard and state-of-the-art binarization techniques. The comparison was done through error assessment. We estimated LAI with the binarized images and used reference data obtained from litter traps for error estimation.

Author version of the manuscript published for Canadian Journal of Forest Research on the web 30 July 2018. DOI: 10.1139/cjfr-2018-0006.
http://www.nrcresearchpress.com/toc/cjfr/0/ja

Description of our method

Background

Our method was based on the EC method by Song et al. (2014), which uses photographs of canopy models with known openness for finding a relationship between OTV and REV2OS. For canopy model photographs, the OTV is the one that produces a binary image with openness near the reference openness. The canopy models used by Song et al. (2014) were made with transparent acrylic plastic sheets partially covered with an opaque black adhesive vinyl sheet. These authors built two types of canopy model, grid canopies and lifelike canopies. Only the latter were used for the development of the EC method. A cylindrical pipe was used to produce back illumination only. The section of one end of the pipe held the canopy model that was photographed from the other end. To obtain diffuse light, a sand-scrubbed acrylic plastic board was attached to the end of the pipe, also helping to secure the canopy model. With this setting, the authors obtained canopy model photographs that showed a circular image with a black margin. For a visual reference of the setting, see Figure 1 by Song et al. (2014). As the authors explained, the circular image filled the area normally occupied by a conventional circular hemispherical image. To measure the auto-EV needed to get the REV2OS, the authors used the sand-scrubbed acrylic plastic board without the canopy model.

Algorithms for auto-EV determination use photodiodes to obtain information of the scene luminance and calculate the EV while considering how the human visual system responds to different wavelengths (Allen and Triantaphillidou 2010). General information about auto-EV determination is available, but its details depend on manufacturers and are trade secrets. Song et al. (2014) applied the EC method to real hemispherical photographs without selecting any specific channel. For canopy model photographs it is easy to set an achromatic scene by making the canopy models black and the light source white, and thus obtaining almost the same information in the three channels.

Author version of the manuscript published for Canadian Journal of Forest Research on the web 30 July 2018. DOI: 10.1139/cjfr-2018-0006.
http://www.nrcresearchpress.com/toc/cjfr/0/ja

Nevertheless, real hemispherical photographs are not achromatic. Therefore, it is not clear how to process the real hemispherical photographs before applying the OTV that was found using the EC method. The method we present here avoids this source of uncertainty.

Gamma correction theory

Digital cameras usually use sRGB as color space, and this standard has been developed to ensure accurate color and tone management (Allen and Triantaphillidou 2010). In an imaging device or system, transfer functions describe the input-to-output relationship. The transfer function of sRGB, known as gamma correction, is very close to a power function with the exponent 1/2.2; it contributes to optimize file size maintaining the perceived image quality when color depth is degraded to 24-bit (Allen and Triantaphillidou 2010). This is why a DN of a born-digital photograph that was encoded in sRGB has a non-linear relationship with luminance (Cescatti 2007, Allen and Triantaphillidou 2010). In HP, dark pixels are considered as backlit plants, light pixels as the sky and grey pixels as the result from the mixture of these two elements. Therefore, a linear relation between object luminance and DN is desired. Equation 1 transforms the corrected value to the original value:

$$DN_{GBC} = 255 \times \left(\frac{DN}{255}\right)^{2.2} \quad (1)$$

where DN is the digital number of a JPEG file in sRGB and DN_{GBC} is the gamma back-corrected DN. It is worth noting that values were not rounded to the nearest integer.

Development

For developing our method, we obtained canopy model photographs replicating the

Author version of the manuscript published for Canadian Journal of Forest Research on the web 30 July 2018. DOI: 10.1139/cjfr-2018-0006.
http://www.nrcresearchpress.com/toc/cjfr/0/ja

195 method by Song et al. (2014) (details can be found in Supplementary material S1). We
196 found the threshold value using the 1-%-optimal-thresholding-range method proposed by
197 Song et al. (2014) but using the gamma back-corrected DN in the blue channel
198 (Equation 1) instead of the original photograph, as Song et al. (2014) did.
199 We found a consistent pattern between openness, threshold value, and the DN of the
200 classes Background and Object. Figure 1 shows the results for the two most closed
201 canopy models and the two most open ones. In both cases, the Background DN was
202 homogeneous. However, in the open canopy model photographs the Object DN had
203 greater heterogeneity than in the closed ones. The difference in number of mixed pixels
204 could produce this discrepancy. In the case of our canopy model photographs, the open
205 ones had a silhouette with more border length than did the closed ones; hence, they had
206 the greatest number of mixed pixels (Song et al. 2014). Therefore, assuming very low
207 multiscattering because of the illumination setting, this threshold assigned the majority of
208 mixed pixels to the Object class. Thus, this threshold behaved as the initial value.
209

Author version of the manuscript published for Canadian Journal of Forest Research on the web 30 July 2018. DOI: 10.1139/cjfr-2018-0006.
http://www.nrcresearchpress.com/toc/cjfr/0/ja

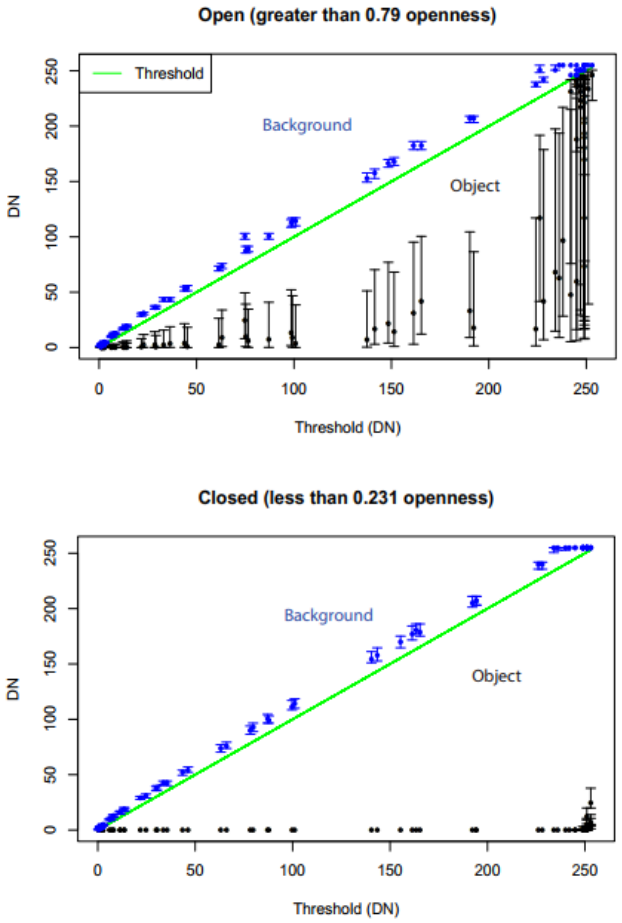

Figure 1. Digital number (DN) extracted from canopy model photographs. Pixels were classified as Background or Object using the threshold obtained with the 1-%-optimal-thresholding-range method proposed by Song et al. (2014). Error bars are the interquartile range. Figure provided in color online.

The relationship between the initial value (IV) and Background DN was approximately linear until saturation (Figure 1). Therefore, a linear model could be fitted and used to estimate the IV using the Background DN. In addition, we introduced a weighting parameter (W) to transform IV in OTV,

$$OTV = a + b \times W \times BG \quad (2)$$

where a and b are the coefficients of the linear model and BG is the Background DN.

Author version of the manuscript published for Canadian Journal of Forest Research on the web 30 July 2018. DOI: 10.1139/cjfr-2018-0006.
http://www.nrcresearchpress.com/toc/cjfr/0/ja

Weighting parameter range must be between 0 and 1, assuming that an OTV must be lower than the IV. The goal of W is to assign the darker mixed pixels to Plant and the lighter to Sky. We assume that this parameter should be 0.5 for ideal scenes with diffuse light, no multiscattering, and no transmission through leaf tissues.

Our method reduces the problem of thresholding to the one of estimating Background DN. If this value is known by any method for each pixel, then OTV can be calculated locally to easily perform a local thresholding. In this paper, a weighting parameter of 0.5 was used as a general approach, assuming the pure plant pixels have 0 DN.

The basic software needed to use the methods presented in this paper were programmed in the R package caiman (Díaz 2016).

Materials and methods for error assessment

Study site and sampling units

Study site (Figure 2) was the Huemules Norte Experimental Unit (42°46′S, 71°29′W) of the National University of Patagonia San Juan Bosco (UNPSJB), located 26 km northwest of Esquel City, Argentina. It is on the mountain Cordón Rivadavia, 1140 m above sea level with a southeast aspect. It has small, east-west oriented undulations with slopes not greater than 26°. These undulations produce zones with north and south aspects at the microscale. The study site has 40 hectares covered with forest of lenga (*Nothofagus pumilio*).

Author version of the manuscript published for Canadian Journal of Forest Research on the web 30 July 2018. DOI: 10.1139/cjfr-2018-0006.
http://www.nrcresearchpress.com/toc/cjfr/0/ja

Figure 2. Real color orthomosaic of the study site. An unmanned aerial system was used to take the photographs. Dots mark the center of the circular plots used as sampling units, which are identified with a number. The red square maps the position where the photographs of the open sky were taken. Figure provided in color online.

At the study site, we selected 10 forest patches (structurally homogeneous regions) to represent the structural variability of the lenga forest. In each forest patch, we set up one circular plot of 10 m radius with 3 litter traps and 4 positions for photograph acquisition (photosite). A photosite was located in the plot center and three in the plot perimeter at 0°, 120°, and 240° azimuth angle. However, if any photosite was near a large tree or under low branches, all the photosites were relocated to avoid these error sources, while maintaining the relative distances between photosites. At each plot, the 3 litter traps were set up using randomly generated azimuth angles and distances from the center of the plot, limiting the distances to between 1 to 9 m to avoid the plot border and overlap of litter traps at the center.

Author version of the manuscript published for Canadian Journal of Forest Research on the web 30 July 2018. DOI: 10.1139/cjfr-2018-0006.
http://www.nrcresearchpress.com/toc/cjfr/0/ja

Reference data

The LAI was measured using litter traps, as was described in the literature (Bouriaud et al. 2003, Pitman 2013). We used litter traps with a mouth diameter of 65 cm and a conic bag of 70 cm depth. One litter trap from plot 6 was omitted because of damage. To discard all but the leaves, the fine materials were discarded using a 3 mm mesh and the coarse materials were discarded by hand. The leaves were dried at 60° C to a constant weight and weighed on a digital scale (to the nearest 0.1 g). To estimate the specific leaf area (SLA), we randomly selected a subsample of 30 leaves (before drying) per litter trap. Leaf area of the subsamples were measured using a desktop scanner (200 dpi). Next, the subsamples were dried at 60° C to a constant weight and weighed on a digital scale (to the nearest 0.0001 g). We calculated the SLA per plot as the simple average. See supplementary material S2 for details.

Hemispherical photograph acquisition

We used the Nikon FC-E9 fisheye converter attached to the Nikon Coolpix 5700 camera. This equipment allowed us to get circular fisheye photographs with nearly equidistant projection. See supplementary material S3 for details about the lens projection function. We acquired hemispherical images of 1490 pixel diameters (180º field of view). We used the camera setting for Coolpix 5400 recommended by Delta-T: white balance in auto, metering in matrix, and image adjustment, saturation, image sharpening, and lens in normal (Delta-T-Devices 2003). All photographs were acquired with ISO-100 and stored in JPEG format.

Our goal was to have a series of photographs taken using a wide range of EVs for each photosite. To that end, we took photographs and evaluated them looking at the preview on the display, starting with the lowest REV that allowed us to interpret some of the canopy silhouette in the preview and incrementing the REV by approximately one stop, repeating until the sky in the preview looked clearly saturated. On February 12, 2014 (summer and leaf-on), we acquired 253 photographs between 19:38 and 21:05

Author version of the manuscript published for Canadian Journal of Forest Research on the web 30 July 2018. DOI: 10.1139/cjfr-2018-0006.
http://www.nrcresearchpress.com/toc/cjfr/0/ja

hours; sunset was at 20:55 hours. The sky was clear, and the air was calm. Making variations in the exposure (mainly the shutter speed, but also the aperture), we took between 3 and 10 photographs per photosite. On May 23, 2014 (fall and leaf-off), we acquired 136 photographs between 17:25 and 18:22 hours; sunset was at 18:24 hours. The sky had broken cirrus clouds and a soft wind was blowing. We repeated the methods used in summer. We took between 3 and 4 photographs per photosite.

To determine the auto-EV for the open sky, we took three photographs in an open area using the fisheye converter attached to the camera set in auto-exposure mode. These pictures are available in our project on the Open Science Framework (Díaz 2017b). The open area was of approximately 60 m radius (Figure 2). The photographs showed the sky free of obstacles between 0° and 70° zenith angle. Below this range, the photographs showed distant mountains. Two of these photographs were taken during the work session and one at the end. Taking a photograph before starting the work session was difficult because of the short time window during dusk and the inconvenience of the spatial arrangement between the plots and the open area (Figure 2). In the next paragraphs we explain how we obtained the REV2OS.

We calculated the EV using Equation 3 (Allen and Triantaphillidou 2011):

$$EV = log_2\left(\frac{N^2}{t}\right) \quad (3)$$

where N is the f-number and t is the shutter speed. In modern cameras, the sensitivity is expressed as ISO speed. To ensure the meaningfulness of the EV comparisons, the same ISO speed was always used.

We used the method splinefun from the R package stats (R Core Team 2017) to perform a natural spline interpolation and obtain a function that used the time and returned the EV for the open sky (EV4OS), which was only valid for the specific photography session under analysis (Figure 3). With the obtained function and the Exif

Author version of the manuscript published for Canadian Journal of Forest Research on the web 30 July 2018. DOI: 10.1139/cjfr-2018-0006.
http://www.nrcresearchpress.com/toc/cjfr/0/ja

312 time (the time when the photograph was taken), we estimated the EV4OS for each
313 photograph taken under the canopy. In addition, we used Equation 3 and the Exif data to
314 calculate the EV for each photograph. Finally, we calculated the REV2OS by subtracting
315 the photograph-EV from the EV4OS.
316

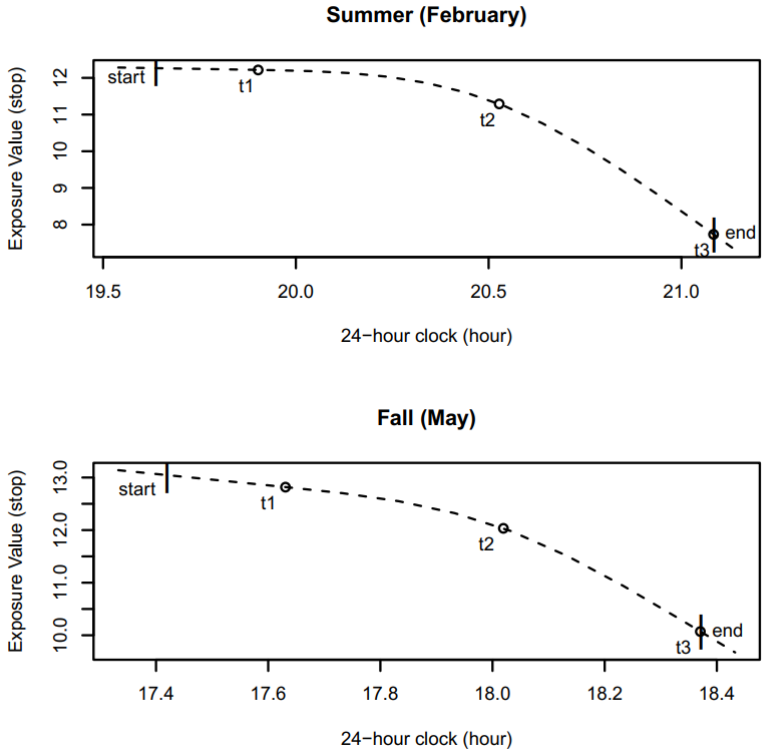

317
318 Figure 3. Natural spline interpolation (broken lines) of the exposure value for the open
319 sky. Dots (t1, t2, and t3) show when photographs of the open sky were taken, “start” and
320 “end” indicate time window used to take all the photographs (ISO-100).
321
322
323 We made classes of REV2OS rounding to the nearest integer. During the leaf-on
324 condition, we obtained 33 photographs per class for the classes 1 to 4 stops. For the
325 classes 0, 1, and 2 stops, we had photographs to estimate PAI in all the plots. For the
326 classes 3, 4, and -1 stops, we had photographs to estimate PAI in 9, 8, and 7 plots,
327 respectively. During the leaf-off condition, we used high shutter speed to avoid the blur
328 that small branches produce when they move with the wind; therefore, we obtained a

329 REV2OS that was mainly negative as an unintended drawback. As a result, the -1 stop
330 class was the only one with photographs in all the photosites, and thus we used only the
331 photographs of this class to calculate WAI.
332 Zhang et al. (2005) suggest 2 stops of REV2OS as the optimal exposure. Therefore,
333 the leaf-off photograph has an incorrect exposure according to Zhang et al. (2005)
334 method. The leaf-on photographs of the 2 stops class and the leaf-off photographs of the
335 -1 stop class are available in our project on the Open Science Framework (Díaz 2017b).

336 Estimation of the sky DN as a previous step for our method

337 Our algorithm for sky DN estimation is iterative. To design it, we envisioned the sky DN
338 as a smooth surface. A leveled plane was used for the first step, as a global thresholding
339 approach, a cone shape for the second step, and an irregular smooth surface for the last
340 step. The second step was based on Lang et al. (2010). These authors manually
341 extracted the DN from gaps and used it for fitting a model of sky radiance. In contrast,
342 we automatically extracted the DN from gaps and used it for fitting a generic statistical
343 model:
344

$$sDN = a + b \times \theta + c \times \theta^2 + d \times sin(\varphi) + e \times cos(\varphi) \quad (4)$$

345
346 where sDN is sky Digital Number; a, b, c, d, and e are coefficients; θ is the zenith angle
347 and φ is the azimuth angle.
348 We selected zenith and azimuth angle as predictor variables based on Wagner
349 (2001), Lang et al. (2010), and Figure 4. Wagner (2001) proposed modelling sky
350 brightness without the azimuth angle, but Figure 1 by Lang et al. (2010) and our Figure 4
351 show some azimuth effect on sky brightness. In some cameras, the vignetting function
352 can change with the aperture (Wagner 2001, Lang et al. 2010), but it does not change in
353 our equipment (see supplementary material S4 for details).
354

Author version of the manuscript published for Canadian Journal of Forest Research on the web 30 July 2018. DOI: 10.1139/cjfr-2018-0006.
http://www.nrcresearchpress.com/toc/cjfr/0/ja

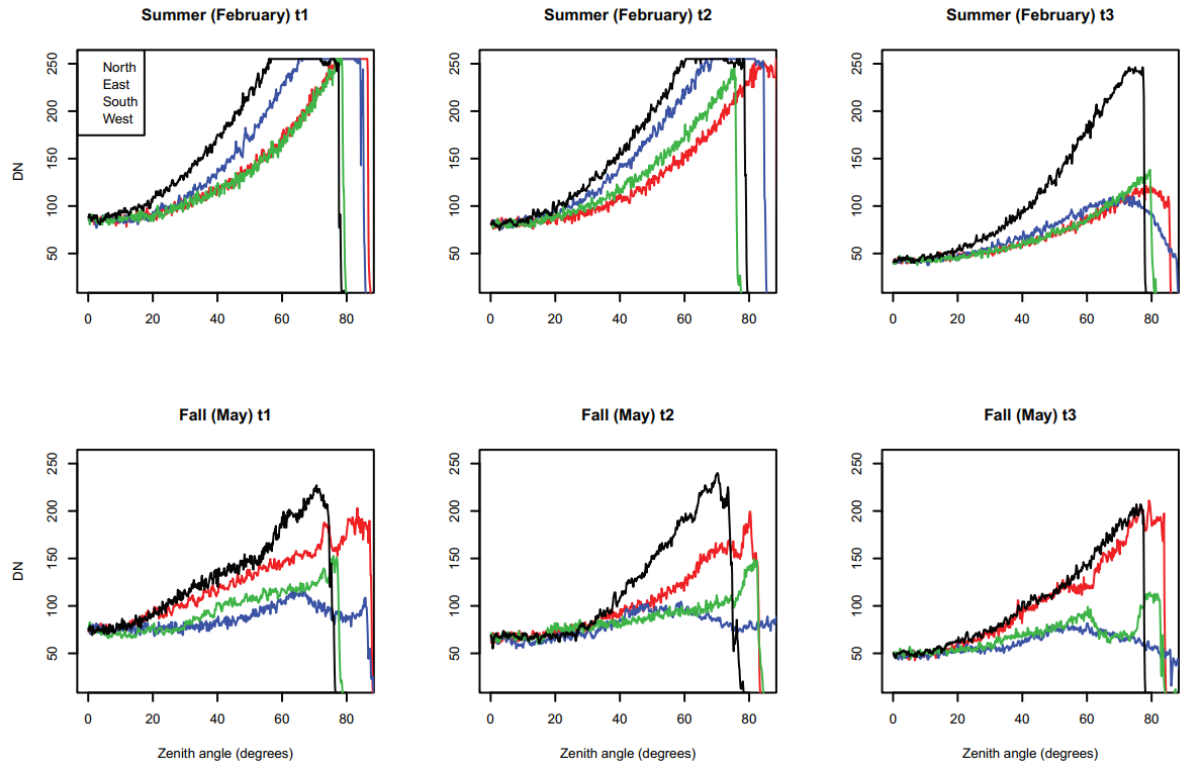

Figure 4. Profiles extracted from hemispherical photographs of the open sky taken in auto-exposure mode. Digital number (DN) extracted from the gamma back-corrected blue channel. Each profile is a straight line oriented to the cardinal points that starts at the zenith and touches the horizon. In the fall photographs, the effect of the azimuth on the relationship between zenith and sky brightness is stronger than in summer photographs, but this effect was also different for the fall photographs, which could be explained by cloud movement. Figure provided in color online.

The algorithm we describe in the next paragraphs could be applied to any channel or synthetic layer, as a brightness layer. We chose to use the blue channel because of its aforementioned advantages. In addition, we applied a back-gamma correction to this channel using Equation 1.

Any available automatic global thresholding could be used for the first step, but we preferred to use our method. To that end, we started by estimating an average value for sky DN. Figure 4 shows that the region between 30° and 60° zenith angle should be

good to find an average value of the sky DN. With all the pixels of this region, the quantile 0.95 was computed. In theory, the maximum should be used because the pure sky pixels should be the brightest, but we used this quantile to avoid extreme values. Next, a working binary image was produced with the global threshold estimated using Equation 2 and W = 0.5.

The second step used the working binary image to extract the sky DN from gaps. Specifically, the quantile 0.95 was computed with the Sky pixels extracted from 5° angular resolution segments. Depending on canopy structure and quality of the working binarized image, some segments had no gap. To fill these voids, data from an asynchronous picture of the open sky was used. The time difference between the available pictures of the open sky and the photograph under analysis was calculated and the picture with less time difference was selected as filling data. Using the portion of the sky in which both filling and extracted data overlapped, the bias between data sources was obtained and used to correct the filling data before it was actually used to fill the voids. Applying a bias to the filling data is a valid approach as Figure 8 from Wagner (2001) shows. Exposure variation shifts sky profiles up or down with minor changes in their form. Figure 1 of supplementary material S5 confirms this effect. In summary, this merged data is the combination of sky DN extracted from gaps with the adjusted DN from a photograph of the open sky.

Next, Equation 4 was fitted using the merged data. To finalize the second step, the fitted model was used to estimate the sky DN for each pixel of the photograph and obtain a refined working binarized image using Equation 2 and W = 0.5.

The last step started by producing new merged data using the refined working binarized image and a method only slightly different than the previous one. With the new merged data, a trend surface was fitted by least-squares using the method surf.ls (np = 6) from the R package spatial (Venables and Ripley 2002). This was the final estimation of sky DN. This algorithm is part of an open source R script that uses methods from the R package caiman along with other R features (Díaz 2017a).

Author version of the manuscript published for Canadian Journal of Forest Research on the web 30 July 2018. DOI: 10.1139/cjfr-2018-0006.
http://www.nrcresearchpress.com/toc/cjfr/0/ja

Binarization methods used to compare with our method

We compared our method against both standard and state-of-the-art binarization techniques. We used the Ridler and Calvard (1978) –isodata– and Nobis and Hunziker (2005) –nh2005– binarization algorithms; specifically, the Hemisfer 2.2 implementations. Hemisfer is proprietary software from the Swiss Federal Institute for Forest, Snow and Landscape Research (WSL). Hemisfer has features for gamma back-correction (GBC) and for regional thresholding. We tested isodata and nh2005 with and without GBC. The regional thresholding implemented in Hemisfer is by ring. With this option, a threshold is automatically calculated for each ring. The number of rings is up to the user. We chose 9 rings of 10° each. All the pixels between 180° field of view (FOV) were used for automatic thresholding.

The EC method was also tested. Because we used different equipment than Song et al. (2014), we calibrated the EC method for our equipment. Details on how the canopy model photographs were taken can be found in Supplementary material S1. All the calculations needed to calibrate the EC method were programed in the R package caiman (Díaz 2016), in the methods getReady4ECM, findOTRs, and getECMfun. The last method is a wrapper for the mle2 method of the R package bbmle (Bolker and R Development Core Team 2017). This method performs a maximum likelihood estimation.

Binarization of the leaf-off photographs

This paper focused on binarization of leaf-on photographs. Plant area index (PAI) could be estimated with the binary images of leaf-on photographs. Because LAI from litter traps was used as reference data, we needed a method to convert PAI to LAI. LAI can be estimated by subtracting the woody area index (WAI) from PAI. We used the leaf-off photographs to estimate WAI. Our goal was to acquire the most accurate WAI with the available set of photographs, which has an incorrect exposure according to the Zhang et al. (2005) method. Therefore, we could not obtain accurate results with isodata and nh2005 algorithms. Unfortunately, the EC method, designed to handle a wide range of

REV2OS, was unreliable for the task (see results section). On the other hand, because most of the literature focused on leaf-on photographs, we had no objective criterion to judge the binarization results. Therefore, we used our own criterion to produce the most accurate results with our methods.

Blue channel histograms of the leaf-off photographs have the peak of the brightest pixels before 100 DN. We took the range between 0 and 75 DN and applied a linear histogram stretching, making this range go from 0 to 255 DN. This made all sky pixels, and probably some mixed pixels, 255 DN. Next, a gamma back-correction was applied with Equation 1. Assuming that all sky pixels were 255 DN, a global threshold was calculated using Equation 2 and W = 0.1. We chose a low value of W because our goal was to classify pure plant pixels.

Estimation of canopy structural variables with HP

Gonsamo et al. (2018) summarized the source, cause, and statistical nature of error sampling and optical errors with GF data, especially near the zenith and the horizon. To avoid errors, we masked out the area with a zenith angle greater than 70° and less than 20° (ring mask). Another source of error was sampling objects beyond plot limits (Gonsamo et al. 2018). Tree crowns beyond plot limits were sampled with the hemispherical photographs we took at the plot perimeter, but also with the ones taken at the plot center. This is not a major concern in forests with low spatial heterogeneity; nevertheless, the natural lenga forests have a gap dynamic that generates high variability at a microscale because gaps are usually created from the destruction of 1 to 3 neighboring trees (López Bernal et al. 2012). Some of our plots were limited by another kind of forest structure. Thus, we evaluated the use of image masking to maximize the correspondence between the canopy area measured with HP and the one measured with litter traps. We tested the azimuthal image masking (sector-ring mask) as shown in Figure 5. Masking was done after the binarization.

Author version of the manuscript published for Canadian Journal of Forest Research on the web 30 July 2018. DOI: 10.1139/cjfr-2018-0006.
http://www.nrcresearchpress.com/toc/cjfr/0/ja

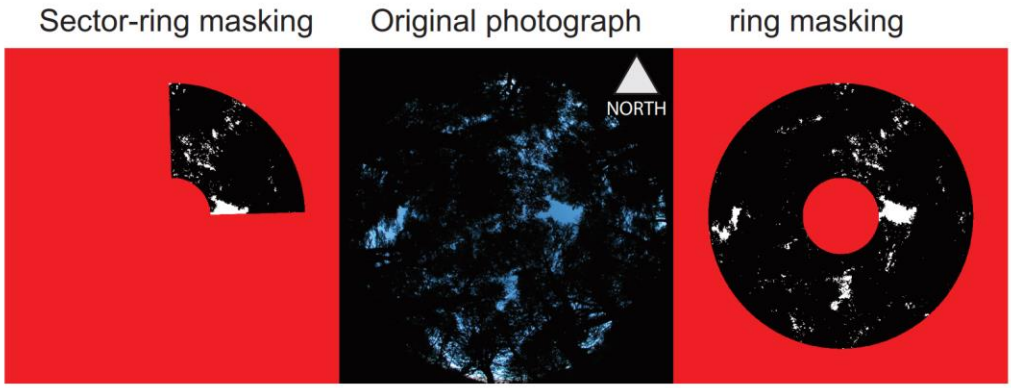

Figure 5. Image masking used to extract GF. Left, binarized image masked with the sector-ring mask; center, unmasked photograph; right, binarized image masked with the ring mask. Zenith angle was restricted between 10° and 70° (left and right). Azimuth was restricted to a range of 45° pointing toward the plot center (left). Figure provided in color online.

We used Hemisfer 2.2 to estimate the effective leaf area index (Le) and the clumping index (Ω). Using LAI for validation has the advantage of including Ω, which is sensitive to error distribution over the hemispherical space (Walter et al. 2003). We calculated LAI by subtracting the woody area index (WAI) from plant area index (PAI). We averaged it to obtain the values per plot. Using the reference data, we calculated the error by plot by subtracting the reference LAI from the estimated LAI.

Hemisfer calculates Ω using only rings with at least two valid segments. A segment with 0 GF (the so-called null-segment) is not a valid one. For LAI calculation, given a ring with 0 GF, Hemisfer assigns to it the GF calculated by changing only one of its pixels from 0 GF to 0.5 GF (Patrick Schleppi, personal communication). The number of segments with 0 GF is affected by the size of the sampling grid. This size also affects the value of both Le and Ω (Gonsamo et al. 2010). To explore what would be the proper angular resolution of the sampling grid for the lenga forest, we tested 2.5°, 5°, and 10°. For this type of forest, it is not clear what algorithm is the best to estimate Le and Ω;

Author version of the manuscript published for Canadian Journal of Forest Research on the web 30 July 2018. DOI: 10.1139/cjfr-2018-0006.
http://www.nrcresearchpress.com/toc/cjfr/0/ja

476 therefore, we tested several. To estimate Le, we used algorithms from Miller (1967),
477 Lang (1987), Norman and Campbell (1989), and Gonsamo et al. (2018), hereafter called
478 M, L, NC, and GA, respectively. To estimate Ω, we used the Lang and Xiang (1986) and
479 Chen and Cihlar (1995) algorithms, hereafter called LX and CC, respectively. The
480 clumping index was used to correct Le and obtain PAI and WAI. Correcting Le produced
481 PAI or WAI depending on whether leaf-on or leaf-off photographs were used.
482 Three angular resolutions, 4 algorithms for Le calculation, 2 algorithms for Ω
483 calculation, 2 masking methods, and several classes of REV produced hundreds of ways
484 to calculate PAI. As a start, we chose a 5° angular resolution, the ring mask, and the 2
485 stops class. Then, for each coupled binarization (leaf-on and leaf-off) we calculated the
486 Root Mean Square Error (RMSE) of 64 combinations of algorithms (8 for leaf-on
487 photographs and 8 for leaf-off photographs). We chose this statistic because we needed
488 a synthesis of the bias and random errors. To find the best combination of algorithms
489 (COA), we counted the number of binarizations per COA that had a RMSE with less than
490 a 5 % discrepancy with the minimum RMSE. We used the count as a score, so that the
491 highest score means the best COA. Stage 1 in Figure 6 shows this methodology
492 schematically.

Author version of the manuscript published for Canadian Journal of Forest Research on the web 30 July 2018. DOI: 10.1139/cjfr-2018-0006.
http://www.nrcresearchpress.com/toc/cjfr/0/ja

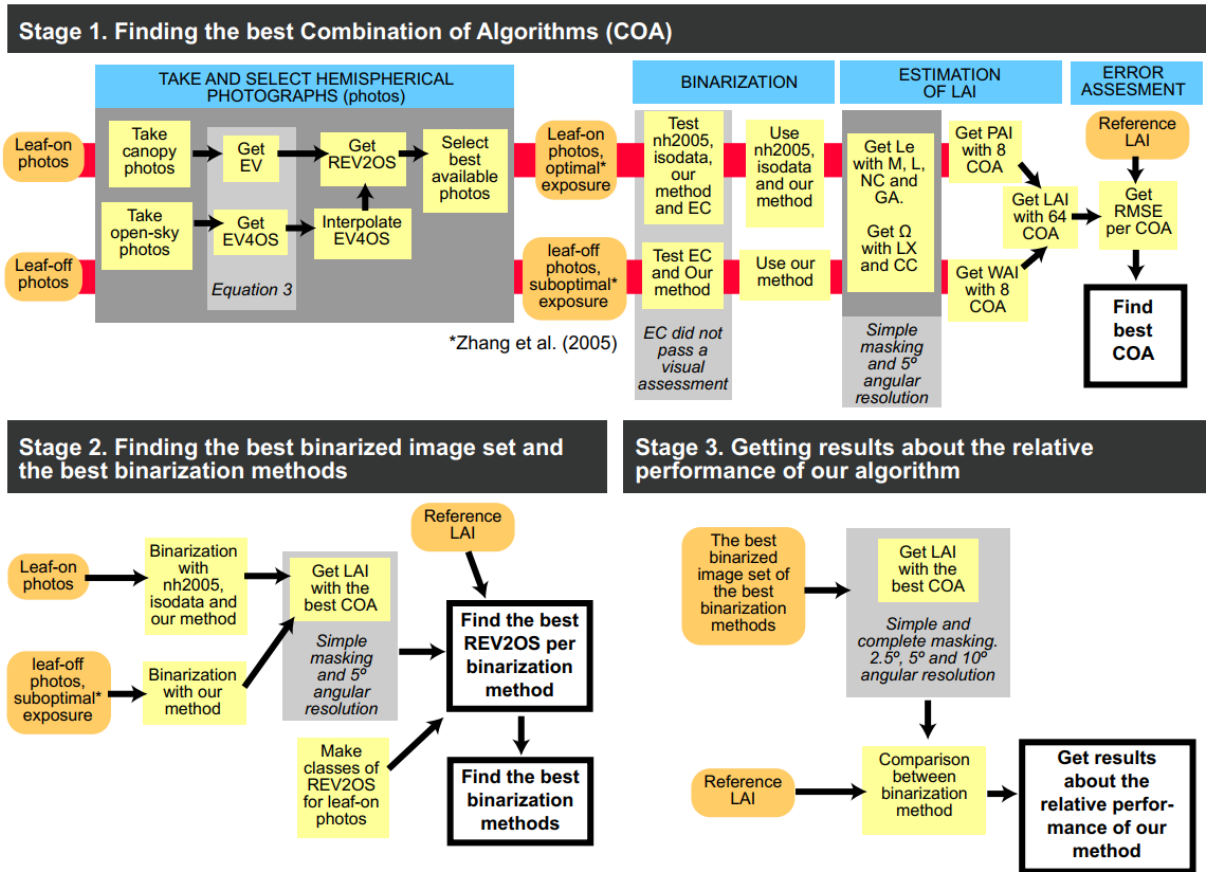

Figure 6. Flow chart of the method used to compare our method against other binarization techniques. EV, exposure value; EV4OS, EV for the open sky; REV2OS, EV relative to the open sky auto-EV; nh2005, isodata, and EC are thresholding methods; LAI, leaf area index; Le, effective LAI; M, L, NC, and GA are algorithm for estimate Le; Ω, clumping index; LX and CC are algorithms to estimate Ω; PAI, plant area index; WAI, woody area index, RMSE, root mean square error. Figure provided in color online.

Performance evaluation for thresholding methods

To determine the best combination of algorithms (COA) to obtain the LAI allowed us to make a straightforward test to find the REV2OS that produced the most accurate binary images per binarization method. Stage 2 in Figure 6 shows this methodology schematically. Knowing the optimal exposure for each binarization method and the best COA for getting LAI, we selected the best binarization methods to determine whether

Author version of the manuscript published for Canadian Journal of Forest Research on the web 30 July 2018. DOI: 10.1139/cjfr-2018-0006.
http://www.nrcresearchpress.com/toc/cjfr/0/ja

changing the angular resolution of the sampling grid and masking method would affect LAI estimation performance. Stage 3 in Figure 6 shows this methodology schematically.

Results

Calibrating our method for the Nikon Coolpix 5700 camera

We took canopy model photographs replicating the method by Song et al. (2014) (details can be found in Supplementary material S1). The REV of the canopy model photographs varied from approximately -4 to 6 stops. We calibrated our method using the gamma back-corrected DN in the blue channel (Equation 1). The linear model fit the data well (Figure 7). The coefficient of the linear model was used with Equation 2 to estimate the optimal threshold value with our method.

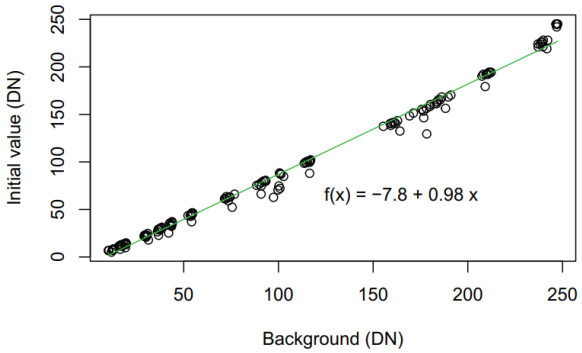

Figure 7. Calibration of our method for the Nikon Coolpix 5700 camera. The data were produced with the canopy model photographs and the 1-%-optimal-thresholding-range method proposed by Song et al. (2014). DN is the digital number, which was gamma back-corrected with Equation 1.

Calibrating the EC method for the Nikon Coolpix 5700 camera

We calibrated the EC method using the average of the three channels of the canopy

Author version of the manuscript published for Canadian Journal of Forest Research on the web 30 July 2018. DOI: 10.1139/cjfr-2018-0006.
http://www.nrcresearchpress.com/toc/cjfr/0/ja

526 hemispherical photographs. The optimal threshold value (OTV) reached a plateau in 2
527 stops. The range from -4.22 to 1.94 stops was used to estimate the coefficients of the
528 function of the EC method. This range included 256 photographs. The data showed a
529 clear tendency and the function of the EC method fit this tendency well (Figure 8). The
530 result of the calibration process is Equation 5,
531

$$OTV = \frac{307}{1 + e^{\frac{-REV - 0.0979}{1.36}}} \quad (5)$$

532
533 where OTV is the optimal threshold value and REV is the EV relative to the reference
534 exposure.
535

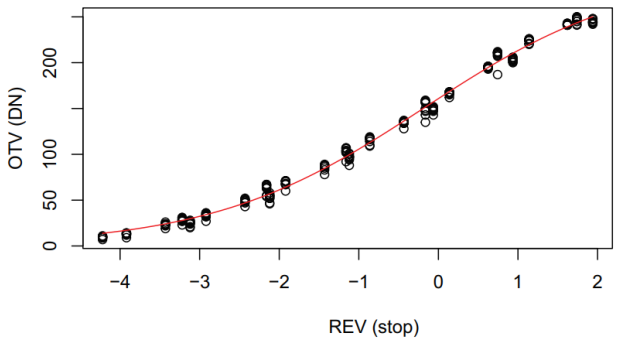

536
537 Figure 8. Function of the ECM method for the Nikon Coolpix 5700. REV is the exposure
538 value relative to the reference exposure (i.e., auto-EV for the open pipe). OTV is the
539 threshold value that produced a binary image with error less than 1 % openness.
540

541 Application of the EC method

542 The application of the EC method on actual hemispherical photographs showed a
543 systematic error. There was uncertainty about how to process a canopy hemispherical
544 photograph before applying the OTV obtained with the EC method. We tried each
545 channel and also calculated the simple average of the three channels and a weighted

Author version of the manuscript published for Canadian Journal of Forest Research on the web 30 July 2018. DOI: 10.1139/cjfr-2018-0006.
http://www.nrcresearchpress.com/toc/cjfr/0/ja

546 average (0.299R + 0.587G + 0.114B) that is used to convert RGB to YUV color space.

547 Any binarization passed the visual assessment, as can be seen in Figure 9.

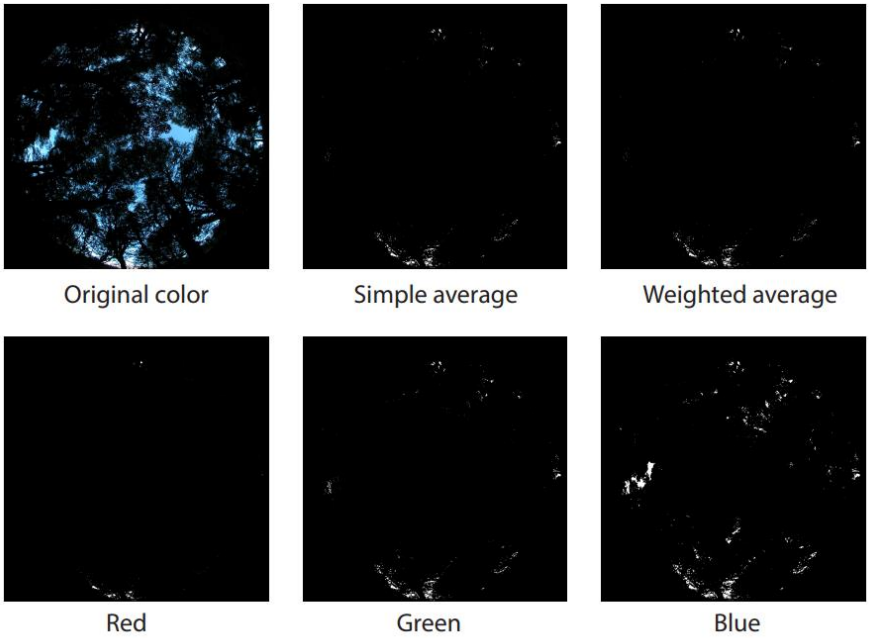

548

549 Figure 9. Example of the error produced by the EC method. The photograph has a
550 REV2OS of 1 stop. The OTV estimated with the EC method was applied to the three
551 channels (Red, Green, and Blue) and to two synthetic layers (Simple average and
552 Weighted average). Figure provided in color online.

553

554 Leaf-off photographs

555 Figure 10 shows examples of how we binarized the leaf-off photographs.

Author version of the manuscript published for Canadian Journal of Forest Research on the web 30 July 2018. DOI: 10.1139/cjfr-2018-0006.
http://www.nrcresearchpress.com/toc/cjfr/0/ja

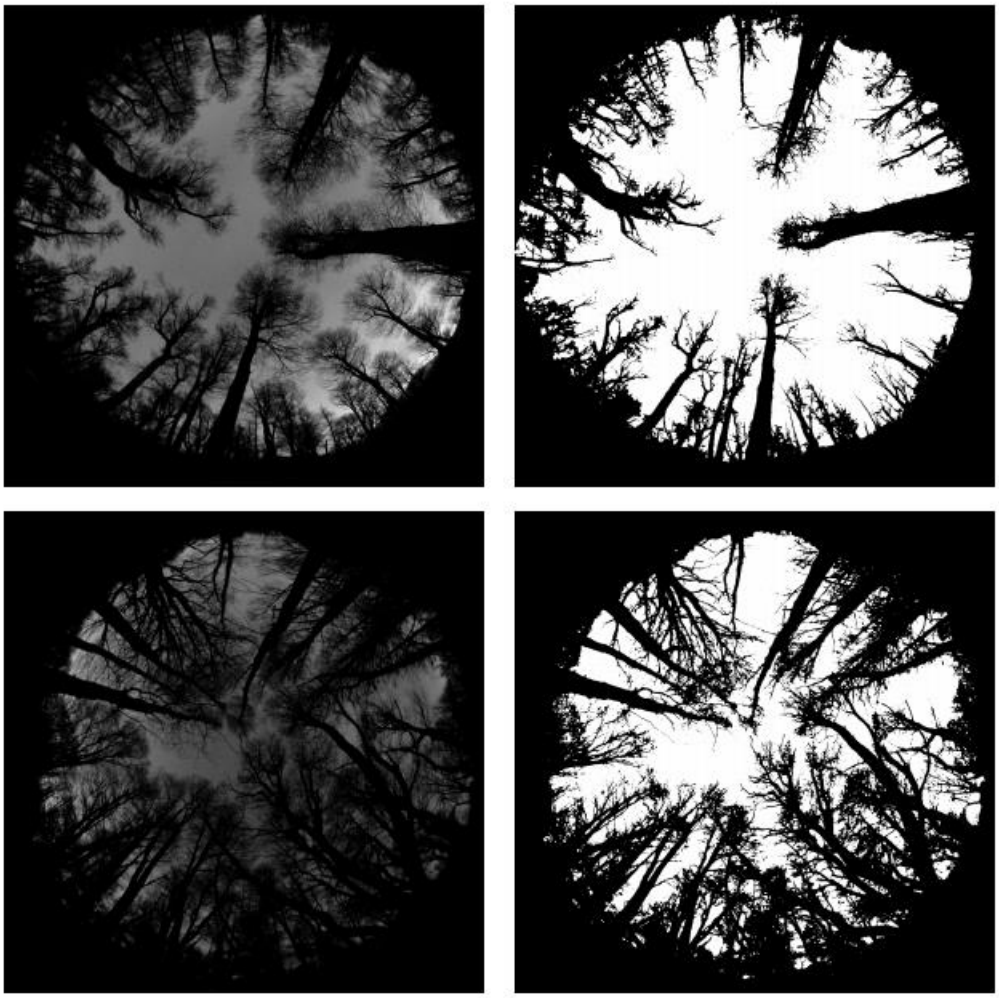

Figure 10. Two examples of binary images used for estimating woody area index. Left, original blue channel of leaf-off photographs. Right, binary images.

Comparison of our method against other binarization techniques

We found 15 good combinations of algorithms (COA) to retrieve LAI with binarized hemispherical photographs of the lenga forest (Table 1). In these COAs, it was clear that the best algorithm to estimate clumping index was LX for summer photographs and CC for fall photographs. Based on this result, we estimated LAI for stage 2 with the M-LX-M-CC COA. The other COAs with the highest score produced similar results (data not shown).

Author version of the manuscript published for Canadian Journal of Forest Research on the web 30 July 2018. DOI: 10.1139/cjfr-2018-0006.
http://www.nrcresearchpress.com/toc/cjfr/0/ja

COA	Score	COA	Score	COA	Score
M-LX-M-CC	7	L-LX-GA-CC	7	NC-LX-L-CC	2
M-LX-L-CC	7	M-LX-NC-CC	5	NC-LX-GA-CC	2
L-LX-NC-CC	7	M-LX-GA-CC	5	L-LX-GA-LX	2
L-LX-M-CC	7	NC-LX-NC-CC	5	M-LX-M-LX	1
L-LX-L-CC	7	NC-LX-M-CC	2	M-LX-L-LX	1

Table 1. Score per combination of algorithms (COA). The COAs not listed here had a frequency equal to zero.

The best binarized image set was produced using the photographs with REV2OS of 2 stops (Figure 11). The performance of both isodata and nh2005 was better at REV2OS of 2 stops. At this REV2OS, the regional version of these algorithms was very similar to their respective global version, except for isodata without gamma back-correction (GBC). For these algorithms, overestimation of LAI was observed after 2 stops and underestimation before it. Our method was among the ones with the best performance and appears to be less sensitive to the REV2OS.

Angular resolution and masking type did not affect the estimation of LAI (Figure 12). We chose 5° angular resolution and the sector-ring mask to assess the relative performance of our method (Figure 13). For optimal exposure, the estimations of the three binarization methods were very similar.

Author version of the manuscript published for Canadian Journal of Forest Research on the web 30 July 2018. DOI: 10.1139/cjfr-2018-0006.
http://www.nrcresearchpress.com/toc/cjfr/0/ja

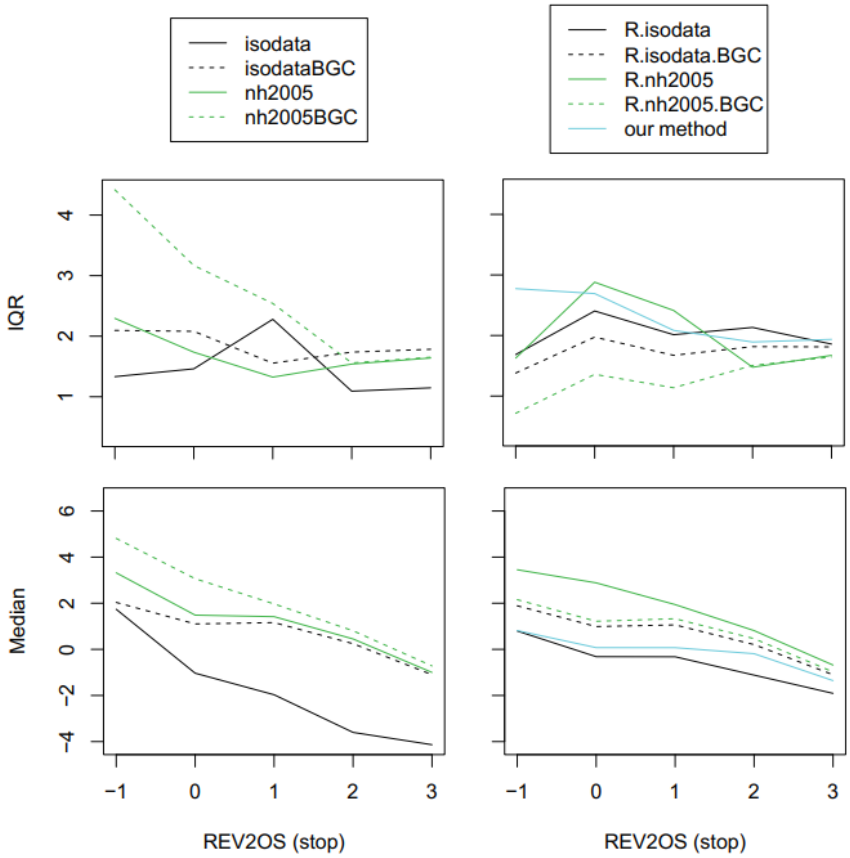

584

585 Figure 11. Error in the estimation of LAI with hemispherical photographs. Left, global
586 thresholding algorithms. Right, regional and local thresholding algorithms. R.* means
587 regional and *.GBC means gamma back-correction. IQR means Interquartile range. The
588 M-LX-M-CC combination of algorithms was used. Figure provided in color online.

589

Author version of the manuscript published for Canadian Journal of Forest Research on the web 30 July 2018. DOI: 10.1139/cjfr-2018-0006.
http://www.nrcresearchpress.com/toc/cjfr/0/ja

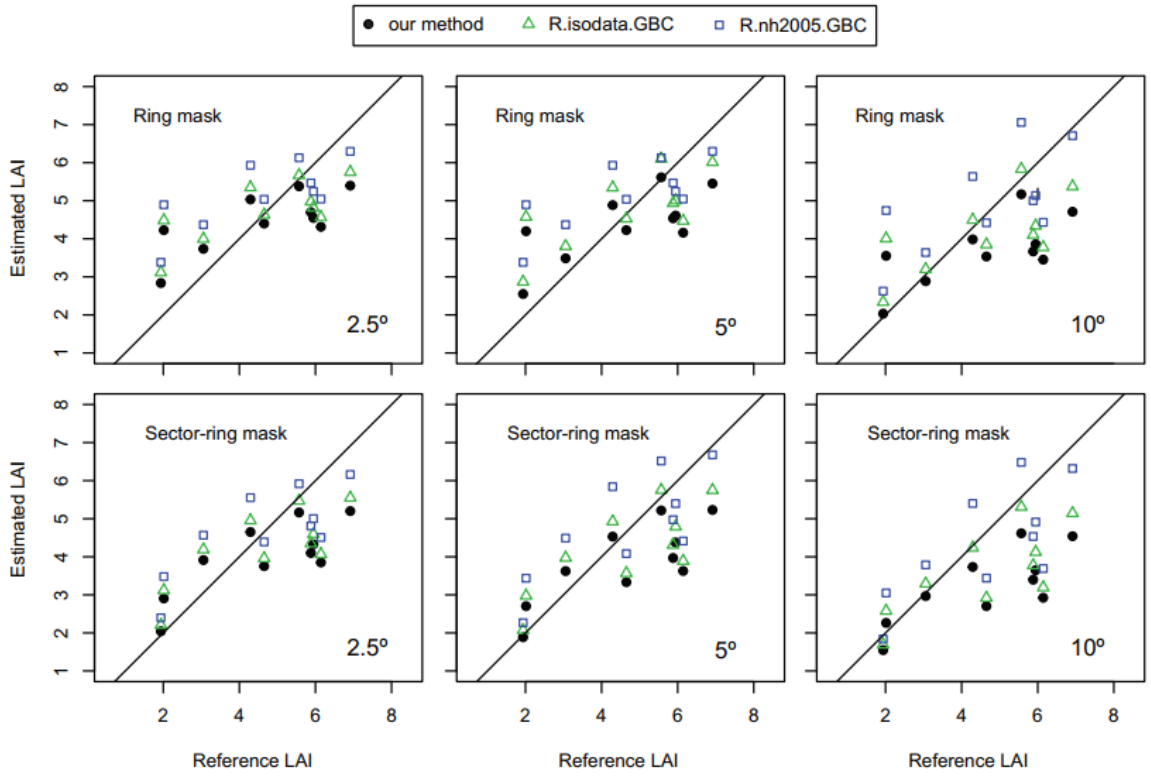

590

591 Figure 12. Effect of angular resolution (2.5°, 5°, and 10°), masking type (ring and sector-
592 ring), and binarization technique (our method, isodata, and nh2005) on the accuracy of
593 LAI estimation. R.* means regional and *.GBC means gamma back-correction. Black
594 lines are the 1:1 relationship. Two stops of REV2OS and the M-LX-M-CC combination of
595 algorithms were used. Figure provided in color online.

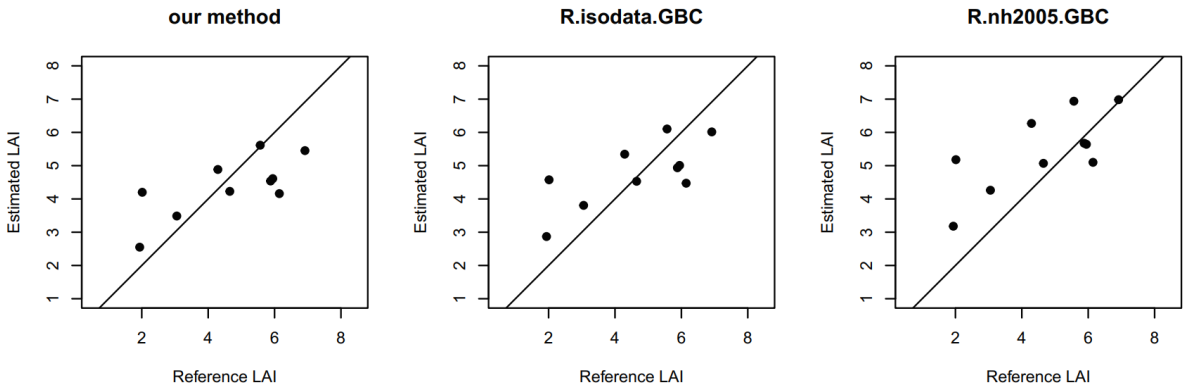

596

597 Figure 13. Comparison of our method against other binarization techniques. R.* means
598 regional and *.GBC means gamma back-correction. Black lines are the 1:1 relationship.
599 Sector-ring making, 5° angular resolution, 2 stops of REV2OS, and the M-LX-M-CC

Author version of the manuscript published for Canadian Journal of Forest Research on the web 30 July 2018. DOI: 10.1139/cjfr-2018-0006.
http://www.nrcresearchpress.com/toc/cjfr/0/ja

600 combination of algorithms were used.

601

602 Discussion

603 Our results confirmed that automatic thresholding algorithms, such as isodata and
604 nh2005, are sensitive to exposure. These algorithms produce an accurate classification
605 in a very narrow range of exposures. Several methods have been proposed to find the
606 optimal exposure. Some authors based on final image appearance to developed
607 methods that did not require above canopy references. For this approach, two major
608 methods were suggested: (1) use of hardware and software of the camera to evaluate
609 saturation in-situ (Leblanc et al. 2005, Beckschäfer et al. 2013) and (2) analysis of image
610 quality in the lab to select the best picture in a series of photographs (Macfarlane 2011).
611 Leblanc et al. (2005) aimed for some saturation in areas without foliage. Beckschäfer et
612 al. (2013) aimed for exposure just before saturation. Macfarlane (2011) selected the
613 least exposed photograph of the series for which the maximum frequency of sky pixels
614 was greater than 200 DN.

615 We demonstrated that the threshold is related to the background DN. Thus, the
616 search for an optimal exposure could be reformulated as a search for an optimal
617 background DN. Indeed, a variation of the approach of Macfarlane (2011) could be easily
618 implemented. Users could take a series of photographs and choose the best photograph
619 using sky DNs as a reference. This is a more objective method than the ones based on
620 exposure because there are several uncertainties about how the photometers work and
621 how they are operated. For example, in Figure 7 of Zhang et al. (2005) the reference sky
622 is approximately 150 DN, which was almost the same DN of our reference sky for the
623 average of the three channels, but the DN was higher for the blue channel.

624 Optimal exposure for the real hemispherical photographs binarized with isodata and
625 nh2005 (Figure 11) is not the same for canopy model photographs (Song et al. 2014).

Author version of the manuscript published for Canadian Journal of Forest Research on the web 30 July 2018. DOI: 10.1139/cjfr-2018-0006.
http://www.nrcresearchpress.com/toc/cjfr/0/ja

Sky heterogeneity could produce this difference. Figure 6 of Zhang et al. (2005) shows a relationship between mean sky DN in the blue channel and REV2OS that shifts from a constant to a decreasing positive rate of change at 2 stops of REV2OS. This shift could be explained by pixel saturation. In a heterogeneous sky, the saturated area starts small and increases with exposure until all pixels are saturated. Saturation is a source of error because of the blooming effect (Thimonier et al. 2010). However, saturation decreases sky heterogeneity. Our Figure 11 shows that automatic thresholding algorithms produce overestimation of LAI up to the optimal exposure, after which, they produce underestimation. Sky heterogeneity appears to be the source of errors before optimal exposure and saturation after optimal exposure. Our method shows results as good as isodata and nh2005, but in a wider range of exposure (0 to 2 REV2OS). We argue that this is because sky heterogeneity was considered in the calculations performed by our method.

Using the EC method, there is not an optimal exposure for canopy model photographs, and the same accuracy could be obtained with a wide range of exposures. Nevertheless, what is true for canopy model photographs was untrue for our real hemispherical photographs. There was uncertainty about how color hemispherical photographs need to be preprocessed. Nevertheless, Song et al. (2014) successfully applied the EC method to real hemispherical photographs. The main difference between their study and ours could be how the reference exposure was measured. Song et al. (2014) measured the reference exposure with an additional camera equipped with an 18 mm lens (approximately 100° of diagonal field of view) pointing to the zenith. In contrast, we used the same fisheye converter and camera that we used for the real canopy photographs. They worked under an overcast sky; therefore, they measured the exposure for the brightness portion of the sky. In contrast, we measured the exposure for almost the entire sky. This case is an example of the drawback of using the REV2OS as a key variable instead of the sky DN.

We hypothesize that the weighting parameter of our method loses importance with

654 modern very high-resolution cameras because, in theory, increasing the camera
655 resolution increases the number of mixed pixels but decreases their percentage. An
656 advantage of our method is its robustness. The accuracy of the results depends mainly
657 on the accuracy of the sky DN estimation. The quality of this estimation can be evaluated
658 with relatively simple methodologies, such as taking samples of pure sky pixels. The
659 method used in the present research to estimate the sky DN used only three
660 photographs of the open sky. By contrast, the most accurate estimation could be
661 produced using photographs simultaneously taken both above and under the canopy
662 with identical equipment and exposure. This alternative prioritizes accuracy at the cost of
663 practicality. It resembles the linear ratio method of Cescatti (2007), but it has the
664 advantage of not using a consumer-oriented camera as a radiometer. Another alternative
665 could be to use different cameras but cross-calibrate them with an empirical function.
666 The above canopy camera could be a low-cost model. For example, Bianchi et al. (2017)
667 tested the use of a fisheye lens and a smartphone camera. Such equipment could be
668 transported and controlled by a drone. The open hardware project flone (http://flone.cc/)
669 is an interesting technology that could do this task. Flone is a low-cost quadcopter that
670 can easily carry a smartphone.
671 The use of an above canopy camera could be of special importance for users in
672 lower latitudes, where the twilight is short. These users must work on days of complete
673 or nearly complete cloud cover, which introduces the problem of accurately represent the
674 variation in sky DN across a single image and between images. However, further
675 research is needed to test our method in this working condition. With good above canopy
676 data, our method can take into account the heterogeneity of the cloudy sky in the
677 calculation of local threshold values.
678 Our results show that our method produces binary images as accurate as the best
679 available automatic thresholding algorithms. One advantage of our method is that it
680 produces good results regardless of the exposure, as long as it was between 0 and 2
681 stops over the open sky auto-exposure. Moreover, knowing of the exact relative

682 exposure is not required. Nevertheless, its main advantage is that it can take full
683 advantage of above canopy photographs using a transparent approach. We consider
684 that our method has the potential of producing an accurate estimation of GF with high
685 angular resolution and becoming a new benchmark.
686

687 ## Acknowledgements

688 We thank Veronica Verano for language and field help, Ariel Neri for lab help, and
689 Agustina Bouza for language help. This work was supported in part by the Argentinian
690 National Agency for the Promotion of Science and Technology through the Scientific and
691 Technological Research Project 3325.
692

693 # References

694 Allen, E., and Triantaphillidou, S. 2011. The manual of photography. *In* 10th edition. *Edited*
695 *by* E. Allen and S. Triantaphillidou. Elsevier, Amsterdam.
696 Beckschäfer, P., Seidel, D., Kleinn, C., and Xu, J. 2013. On the exposure of hemispherical
697 photographs in forests. iForest - Biogeosciences For. **6**(4): 228–237.
698 doi:10.3832/ifor0957-006.
699 Bianchi, S., Cahalan, C., Hale, S., and Gibbons, J.M. 2017. Rapid assessment of forest
700 canopy and light regime using smartphone hemispherical photography. Ecol. Evol.
701 (September): 10556–10566. doi:10.1002/ece3.3567.
702 Bolker, B., R Development Core Team. 2017. bbmle: Tools for General Maximum Likelihood
703 Estimation. R package version 1.0.20. https://CRAN.R-project.org/package=bbmle
704 [accessed 17 April 2018].
705 Bouriaud, O., Soudani, K., and Bréda, N. 2003. Leaf area index from litter collection : impact
706 of specific leaf area variability within a beech stand. Can. J. Remote Sens. **29**(3): 371–
707 380.

708 Cescatti, A. 2007. Indirect estimates of canopy gap fraction based on the linear conversion
709 of hemispherical photographs Methodology and comparison with standard thresholding
710 techniques. Agric. For. Meteorol. **143**(1–2): 1–12. doi:10.1016/j.agrformet.2006.04.009.
711 Chen, J.M., and Cihlar, J. 1995. Quantifying the effect of canopy architecture on optical
712 measurements of leaf area index using two gap size analysis methods. IEEE Trans.
713 Geosci. Remote Sens. **33**(3): 777–787. doi:10.1109/36.387593.
714 Delta-T-Devices. 2003. User Manual for the Self Levelling Mount type SLM5. Available from
715 http://www.delta-t.co.uk/wp-content/uploads/2016/11/SLM5-Hemiview-Self-Levelling-
716 Mount-UM.pdf [accessed 17 April 2018].
717 Díaz, G.M. 2016. caiman: Canopy Image Analysis. Available from
718 https://github.com/GastonMauroDiaz/caiman [accessed 7 January 2018].
719 Díaz, G.M. 2017a. Model-based local thresholding algorithm. Available from
720 https://goo.gl/zygWDN [accessed 7 January 2018].
721 Díaz, GM. 2017b. Replication files for the paper Model-based local thresholding for canopy
722 hemispherical photography. Open Science Framework. Available from
723 https://osf.io/kpbrv [accessed 7 January 2018].
724 Díaz, G.M., and Lencinas, J.D. 2015. Enhanced Gap Fraction Extraction From
725 Hemispherical Photography. IEEE Geosci. Remote Sens. Lett. **12**(8): 1784–1789.
726 doi:10.1109/LGRS.2015.2425931.
727 Gonsamo, A., Walter, J.M., and Pellikka, P. 2010. Sampling gap fraction and size for
728 estimating leaf area and clumping indices from hemispherical photographs. Can. J. For.
729 Res. **40**(8): 1588–1603. doi:10.1139/X10-085.
730 Gonsamo, A., Walter, J.M., Chen, J.M., Pellikka, P., and Schleppi, P. 2018. A robust leaf
731 area index algorithm accounting for the expected errors in gap fraction observations.
732 Agric. For. Meteorol. 248(September 2017): 197–204.
733 doi:10.1016/j.agrformet.2017.09.024.
734 Jonckheere, I., Fleck, S., Nackaerts, K., Muys, B., Coppin, P., Weiss, M., and Baret, F. 2004.
735 Review of methods for in situ leaf area index determination Part I. Theories, sensors

736 and hemispherical photography. Agric. For. Meteorol. **121**(1–2): 19–35.
737 doi:10.1016/j.agrformet.2003.08.027.
738 Jonckheere, I., Nackaerts, K., Muys, B., and Coppin, P. 2005. Assessment of automatic gap
739 fraction estimation of forests from digital hemispherical photography. Agric. For.
740 Meteorol. **132**(1–2): 96–114. doi:10.1016/j.agrformet.2005.06.003.
741 Lang, A.R.G. 1987. Simplified estimate of leaf area index from transmittance of the sun's
742 beam. Agric. For. Meteorol. **41**: 179–186.
743 Lang, A.R.G., and Xiang, Y. 1986. Estimation of leaf area index from transmission of direct
744 sunlight in discontinuous canopies. Agric. For. Meteorol. **37**(3): 229–243.
745 doi:10.1016/0168-1923(86)90033-X.
746 Lang, M., Kuusk, A., Mõttus, M., Rautiainen, M., and Nilson, T. 2010. Canopy gap fraction
747 estimation from digital hemispherical images using sky radiance models and a linear
748 conversion method. Agric. For. Meteorol. **150**(1): 20–29.
749 doi:10.1016/j.agrformet.2009.08.001.
750 Leblanc, S.G., Chen, J.M., Fernandes, R.A., Deering, D., and Conley, A. 2005. Methodology
751 comparison for canopy structure parameters extraction from digital hemispherical
752 photography in boreal forests. Agric. For. Meteorol. **129**(3–4): 187–207.
753 doi:10.1016/j.agrformet.2004.09.006.
754 López Bernal, P.M., Defossé, G.E., Quinteros, P.C., and Bava, J.O. 2012. Sustainable
755 Management of Lenga (Nothofagus pumilio) Forests Through Group Selection System.
756 *In* Sustainable Forest Management - Current Research. *Edited by* J.M. Garcia and J.J.
757 Diez Casero. INTECH. pp. 45–66.
758 Macfarlane, C. 2011. Classification method of mixed pixels does not affect canopy metrics
759 from digital images of forest overstorey. Agric. For. Meteorol. **151**(7): 833–840. Elsevier
760 B.V. doi:10.1016/j.agrformet.2011.01.019.
761 Macfarlane, C., Ryu, Y., Ogden, G.N., and Sonnentag, O. 2014. Digital canopy photography:
762 Exposed and in the raw. Agric. For. Meteorol. **197**: 244–253. Elsevier B.V.
763 doi:10.1016/j.agrformet.2014.05.014.

764 Masek, J.G., Hayes, D.J., Joseph Hughes, M., Healey, S.P., and Turner, D.P. 2015. The role
765 of remote sensing in process-scaling studies of managed forest ecosystems. For. Ecol.
766 Manage. **355**: 109–123. Elsevier B.V. doi:10.1016/j.foreco.2015.05.032.
767 Miller, J.B. 1967. A formula for average foliage density. Aust. J. Bot. **15**: 141–144. Available
768 from http://www.publish.csiro.au/paper/BT9670141.htm.
769 Newnham, G.J., Armston, J.D., Calders, K., Disney, M.I., Lovell, J.L., Schaaf, C.B., Strahler,
770 A.H., and Danson, F.M. 2015. Terrestrial Laser Scanning for Plot-Scale Forest
771 Measurement. Curr. For. Reports **1**(4): 239–251. doi:10.1007/s40725-015-0025-5.
772 Nikon. 2018. Understanding ISO Sensitivity. Available from
773 https://www.nikonusa.com/en/learn-and-explore/a/tips-and-techniques/understanding-
774 iso-sensitivity.html [accessed 26 March 2018].
775 Nobis, M., and Hunziker, U. 2005. Automatic thresholding for hemispherical canopy-
776 photographs based on edge detection. Agric. For. Meteorol. **128**(3–4): 243–250.
777 doi:10.1016/j.agrformet.2004.10.002.
778 Norman, J.M., and Campbell, G. 1989. Canopy structure. *In* Plant physiological ecology:
779 field methods and instrumentation. *Edited by* R. Pearcy, J. Ehleringer, H. Mooney, and
780 P. Rundel. Chapman and Hall, New York. pp. 301–325.
781 Pitman, R.M. 2013. Litterfall—Biomass, Chemistry, Leaf Area, and Links with Wider
782 Ecosystem Functioning. In Forest Monitoring Methods for terrestrial investigations in
783 Europe with an overview of North America and Asia. Edited by M. Ferretti and R.
784 Fischer. pp. 251–264. doi:10.1016/B978-0-08-098222-9.00014-5.
785 R Core Team. 2017. R: A Language and Environment for Statistical Computing. Vienna,
786 Austria. Available from https://www.r-project.org/.
787 Schindelin, J., Arganda-Carreras, I., Frise, E., Kaynig, V., Longair, M., Pietzsch, T.,
788 Preibisch, S., Rueden, C., Saalfeld, S., Schmid, B., Tinevez, J.-Y., White, D.J.,
789 Hartenstein, V., Eliceiri, K., Tomancak, P., and Cardona, A. 2012. Fiji: an open-source
790 platform for biological-image analysis. Nat. Methods **9**(7): 676–82.
791 doi:10.1038/nmeth.2019.

792 Ridler, T., and Calvard, S. 1978. Picture thresholding using an iterative selection method.
793 IEEE Trans. Syst. Man Cybern. **8**(8): 260–263.
794 Schleppi, P., Thimonier, A., and Walthert, L. 2011. Estimating leaf area index of mature
795 temperate forests using regressions on site and vegetation data. For. Ecol. Manage.
796 **261**(3): 601–610. Elsevier B.V. doi:10.1016/j.foreco.2010.11.013.
797 Song, G.-Z.M., Doley, D., Yates, D., Chao, K.-J., and Hsieh, C.-F. 2014. Improving accuracy
798 of canopy hemispherical photography by a constant threshold value derived from an
799 unobscured overcast sky. Can. J. For. Res. **44**(1): 17–27. doi:10.1139/cjfr-2013-0082.
800 Thimonier, A., Sedivy, I., and Schleppi, P. 2010. Estimating leaf area index in different types
801 of mature forest stands in Switzerland: a comparison of methods. Eur. J. For. Res.
802 **129**(4): 543–562. doi:10.1007/s10342-009-0353-8.
803 Venables, W.N., and Ripley, B.D. 2002. Modern Applied Statistics with S. In 4th edition.
804 Springer, New York. Available from http://www.stats.ox.ac.uk/pub/MASS4/.
805 Wagner, S. 1998. Calibration of grey values of hemispherical photographs for image
806 analysis. Agric. For. Meteorol. 90(1/2): 103–117.
807 Wagner, S. 2001. Relative radiance measurements and zenith angle dependent
808 segmentation in hemispherical photography. Agric. For. Meteorol. **107**(2): 103–115.
809 doi:10.1016/S0168-1923(00)00232-X.
810 Wagner, S., and Hagemeier, M. 2006. Method of segmentation affects leaf inclination angle
811 estimation in hemispherical photography. Agric. For. Meteorol. **139**(1–2): 12–24.
812 doi:10.1016/j.agrformet.2006.05.008.
813 Walter, J.-M.N., Fournier, R.A., Soudani, K., and Meyer, E. 2003. Integrating clumping
814 effects in forest canopy structure : an assessment through hemispherical photographs.
815 Can. J. Remote Sens. **29**(3): 388–410.
816 Yamamoto, K., Kobayashi, K., Nonoda, T., Inoue, A., and Mizoue, N. 2010. Effect of settings
817 of digital fisheye photography to estimate relative illuminance within forest under low
818 light conditions. J. For. Res. **15**(5): 283–288. doi:10.1007/s10310-010-0189-6.

819 Zhang, Y., Chen, J.M., and Miller, J.R. 2005. Determining digital hemispherical photograph
820 exposure for leaf area index estimation. Agric. For. Meteorol. **133**: 166–181. Available
821 from http://linkinghub.elsevier.com/retrieve/pii/S0168192305001917.
822
823

Author version of the manuscript published for Canadian Journal of Forest Research on the web 30 July 2018. DOI: 10.1139/cjfr-2018-0006.
http://www.nrcresearchpress.com/toc/cjfr/0/ja

Supplementary material

The present supplementary material is related to the article entitled “Model-based local thresholding for canopy hemispherical photography,” by Gastón Mauro Díaz and José Daniel Lencinas.

S1

Taking canopy model photographs

We used the Nikon FC-E9 fisheye converter attached to the Nikon Coolpix 5700 camera. Figure 1 shows the materials and setup used to take the canopy model photographs. These photographs were used to calibrate the EC method and to develop our method. Figure 2 from the article by Song et al. (2014) shows that given a set of models with the same openness, the ones with the gaps of smaller sizes are the most sensitive to an optimal threshold. This result makes sense because, in this context, small gaps mean a greater number of mixed pixels, which are harder to classify than pure pixels. We chose to design canopy models with small squared gaps, aiming to cover the full openness range with 0.1 intervals. Nine canopy models (Table 1) were designed with Adobe Illustrator CC 2017, using mainly the Blend tool. One design constraint was a minimum wall width of 0.5 mm, because of the laser cutting machine (SHC9060, Sierra) used to produce the models. The models were made with 3 mm medium density fiberboard (Figure 1A). The files needed to replicate this methodology are in our project on Open Science Framework (Díaz 2017). After the cut, they were darkened with artist´s black oil paint, diluted with turpentine. To avoid errors because of the thickness of the canopy models, the models were set to vertical with a plumb-bob and the optical axis of the camera was set to horizontal with a tripod level (Figure 1B, C, D, F, and G). We used the maximum zoom in (70 mm of 35 mm equivalent focal

847 length). This zoom minimizes the vignetting effect, as Song et al. (2014) indicate, but also
848 diminishes perspective distortion and facilitates the comparison between the designed
849 openness of the canopy models and the one photographed. As a light source, we used a 38
850 cm sided cubic shaped lightbox with two 30 cm LED-diffuse-light-strips on the top-front of the
851 box (Foldio 2, Orangemonkie. Figure 1, E). We did not use the sand-scrubbed acrylic plastic
852 used by Song et al. (2014) because our light source was diffuse. The only illumination
853 source was the lightbox. We adjusted the distance between the canopy model and the
854 camera to get a circular image of approximately 1550 pixels in diameter, the distance was
855 1.3 m (Figure 1, G).

Author version of the manuscript published for Canadian Journal of Forest Research on the web 30 July 2018. DOI: 10.1139/cjfr-2018-0006.
http://www.nrcresearchpress.com/toc/cjfr/0/ja

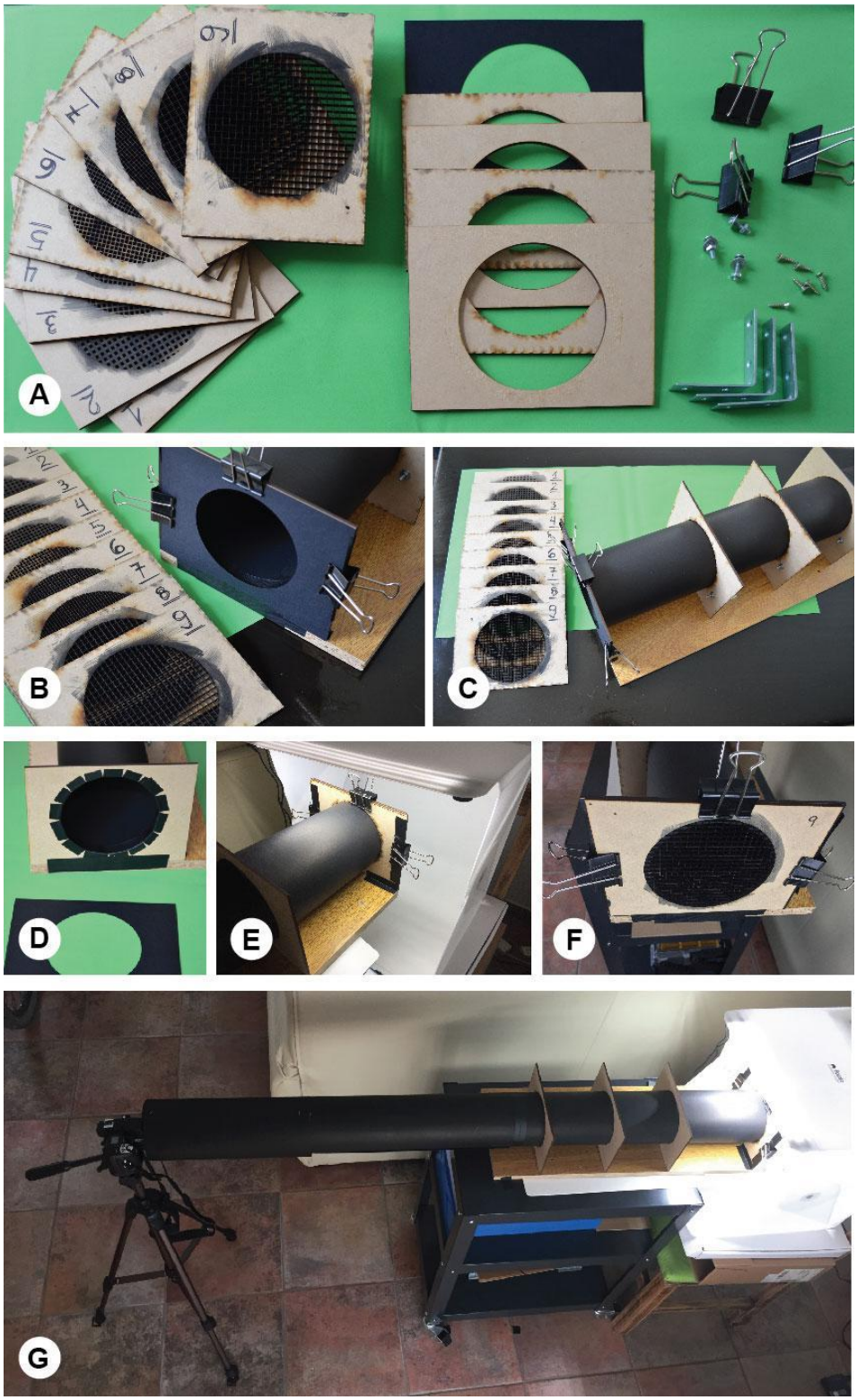

Figure 1. Materials used to take the photographs needed to calibrate the EC method and to develop our method. A) Main components: left, canopy models; right, pieces to support the pipe made of black cardboard. B, C, and D) How the pipe was supported. E) Setup of the light source. F) Canopy model mounted on the pipe end. G) Overall view of the setup.

Author version of the manuscript published for Canadian Journal of Forest Research on the web 30 July 2018. DOI: 10.1139/cjfr-2018-0006.
http://www.nrcresearchpress.com/toc/cjfr/0/ja

861

862 Table 1. Characteristics of the 9 grid canopy models.

Squared gap side (mm)	Wall width (mm)	Openness
2.5	4.7	0.121
2.5	2.7	0.231
2.5	2	0.309
2.5	1.5	0.391
2.5	1.1	0.482
2.5	0.75	0.592
2.5	0.5	0.694
5.0	0.625	0.79
5.0	0.5	0.826

863

864 We used the camera setting for the Coolpix 5400 recommended by Delta-T: white
865 balance in auto, metering in matrix and image adjustment, saturation, image sharpening,
866 and lens in normal (Delta-T-Devices 2003). All photographs were acquired with ISO-100 and
867 stored in JPEG format. The reference auto-EV (i.e., the auto-EV for the open pipe) was
868 influenced by the black margin because the matrix mode meters several areas of the frame
869 to produce the optimal exposure for the whole image. This metering mode is usually the
870 default and the one used by Song et al. (2014). Because the margin of the real canopy
871 photograph was more homogeneously black than the margin of the canopy hemispherical
872 photographs, we adjusted a linear function to correct the auto-EV for the open sky. To that
873 end, we used the lightbox to take photographs with seven light intensities. The coefficient of
874 determination (R^2) was 0.9997. The equation is $f(x) = 0.7970 + 0.9797\ x$.

875 Using four different illumination intensities, we took a total of 343 photographs,
876 approximately 85 photographs per intensity. We started with the highest underexposure that
877 allowed us to interpret some of the grid silhouettes in the preview on the camera display.
878 Then, we slowed shutter speed step by step, taking a photograph each time, and repeating
879 until the preview appeared clearly saturated. A sample of the photographs is available in our
880 project on Open Science Framework (Díaz 2017).

Author version of the manuscript published for Canadian Journal of Forest Research on the web 30 July 2018. DOI: 10.1139/cjfr-2018-0006.
http://www.nrcresearchpress.com/toc/cjfr/0/ja

References

Delta-T-Devices. 2003. User Manual for the Self Levelling Mount type SLM5. Available from http://www.delta-t.co.uk/wp-content/uploads/2016/11/SLM5-Hemiview-Self-Levelling-Mount-UM.pdf [accessed 17 April 2018].

Díaz, GM. 2017. Replication files for the paper Model-based local thresholding for canopy hemispherical photography. Open Science Framework. Available from https://osf.io/kpbrv [accessed 7 January 2018].

Song, G.-Z.M., Doley, D., Yates, D., Chao, K.-J., and Hsieh, C.-F. 2014. Improving accuracy of canopy hemispherical photography by a constant threshold value derived from an unobscured overcast sky. Can. J. For. Res. **44**(1): 17–27. doi:10.1139/cjfr-2013-0082.

S2

Table 1. Reference data. LAI and SLA (cm2/g) per plot, mean and range.

Plot	LAI	Range (LAI)	SLA	Range (SLA)
9	1.94	0.03	134	11.0
6	2.01	0.63	144	12.2
10	3.05	0.37	139	13.4
8	4.29	1.90	156	10.7
4	4.65	1.31	157	27.2
5	5.57	0.53	169	11.1
1	5.88	1.40	157	9.1
3	5.95	1.59	164	19.6
2	6.14	0.55	164	8.3
7	6.92	1.39	175	8.4

S3

Validation of the lens projection function for the Nikon FC-E9 converter

The Nikon Coolpix 5700 is a camera manufactured in the early 2000´s. The FC-E9 is a

converter designed to be attached in front of the lens of several cameras of the Coolpix series, including the 5700. Delta-T manufactured a Self Levelling Mount (SLM5) for the FC-E9 and Coolpix cameras. In the user manual for the SLM5, we found the lens equation coefficients for the FC-E9 (Delta-T-Devices 2003). The same coefficients are available in Hemisfer software. For modelling the lens projection, Hemisfer uses the same method as HemiView, which is the software by Delta-T. These software packages define the relative radius (R) as the distance to the optical center divided by the radius of the horizon circle. Delta-T reported 190° FOV for the FC-E9, so the perimeter of the circular image is not the horizon. Using the published lens function, we obtained R at 95°. We measured 786 pixels from the optical center to the perimeter of the circular image. This value divided by R at 95° is the radius in pixels for R equal one, which is 745 pixels. We performed a lens calibration to validate the published coefficients and the radius in pixels at the horizon.

We set marks on a corner, where the wall meets the ceiling. These marks were set aligned and at approximately 6 cm from each other. The corner was scanned with a Faro Focus^{3D} X 130, using maximum quality and resolution. The scanner was located 1 m from the wall and 1.3 m from the ceiling. This produced a leveled point cloud with accuracy of approximately 1 mm. We used Faro Scene 6.0 software to process the scan and to extract the cartesian coordinates of the marks. We took a hemispherical photograph of the corner, pointing the optical center to the zenith. The front of the lens was in the same position as the scanner mirror, but at 1 m from the ceiling instead of 1.3 m. This difference was considered in calculations. The coordinate transformations were conducted with the R Package pracma (Borchers 2017). The marks were manually located in the photograph using Fiji software (Schindelin et al. 2012). A total of 32 points were located, 14 corresponding to the ceiling and 18 to the wall. The maximum zenith angle was 93.9º and the minimum 14.5º. The model was fitted with the R package stats (R Core Team, 2017).

Equation 1 was fitted using the radius in pixels (residual standard error: 0.91) and Equation 2 was fitted using the relative radius (residual standard error: 0.0012). The two models require a zenith angle (θ) in radians.

925

$$Radius = 488.5 \times \theta + 23.5 \times \theta^2 + 21.4 \times \theta^3 \quad (1)$$

$$R = 0.6581 \times \theta + 0.03159 \times \theta^2 - 0.02881 \times \theta^3 \quad (2)$$

926

927 Using Equation 2, we estimated a FOV of 193º and 742 pixels radius at the 90º zenith
928 angle, values very close to the published ones. Therefore, all calculations were completed
929 with the published values.

930

931 References

932 Borchers, H.W. 2017. pracma: Practical Numerical Math Functions. R package version
933 2.0.7. https://CRAN.R-project.org/package=pracma [accessed 17 April 2018].
934 Delta-T-Devices. 2003. User Manual for the Self Levelling Mount type SLM5. Available from
935 http://www.delta-t.co.uk/wp-content/uploads/2016/11/SLM5-Hemiview-Self-Levelling-
936 Mount-UM.pdf [accessed 17 April 2018].
937 R Core Team. 2017. R: A language and environment for statistical computing. R Foundation
938 for Statistical Computing, Vienna, Austria. URL https://www.R-project.org/.
939 Schindelin, J., Arganda-Carreras, I., Frise, E., Kaynig, V., Longair, M., Pietzsch, T.,
940 Preibisch, S., Rueden, C., Saalfeld, S., Schmid, B., Tinevez, J.-Y., White, D.J.,
941 Hartenstein, V., Eliceiri, K., Tomancak, P., and Cardona, A. 2012. Fiji: an open-source
942 platform for biological-image analysis. Nat. Methods **9**(7): 676–82.
943 doi:10.1038/nmeth.2019.

Author version of the manuscript published for Canadian Journal of Forest Research on the web 30 July 2018. DOI: 10.1139/cjfr-2018-0006.
http://www.nrcresearchpress.com/toc/cjfr/0/ja

S4

Measuring the vignetting effect in the Nikon FC-E9 converter attached to the Nikon Coolpix 5700 camera

The vignetting effect could be modeled with a function for each f-number (Wagner 2001) or with a single function that includes f-number in the input (Lang et al. 2010). In the former approach, the functions need to explain the variation in the relative brightness with the zenith angle, which could be different for each aperture. If the same radiance comes from any direction, the reference brightness is what corresponds to the zenith, assuming a leveled camera. We found that the main difficulty of measuring the vignetting effect was ensuring uniform radiance. Lang et al. (2010) used a photometric sphere, which is probably the best equipment to perform this task, but we did not have access to this equipment. As an alternative, we followed the method of Wagner (2001). This author set a focal light source near the focal point of the lens, arranged white paper discs equidistant to the light source, and placed all the disks facing to the light source. To replicate this method, we used a squared board of 60 by 60 cm, in which we traced a quarter of a circle. Following the perimeter of the arc, we placed a white paper strip perpendicular to the board and a candle in the corner of the board used as the center of the circle. We also tested a conventional bulb instead of the candle, but the results (not shown here) were of lower quality than using the candle. In a room with the candle as the only light source, the board was leveled, and the camera focal point was set below the light source and with the optical axis parallel to the side of the board. Thus, the optical center did not point to the zenith. For simplicity's sake, hereafter, we use the term zenith angle to match that which we used during the operation of the camera in the forest.

We took one photograph for each aperture using auto-exposure with aperture priority and ISO-100. A script for extracting the brightness along the zenith angle was developed.

Author version of the manuscript published for Canadian Journal of Forest Research on the web 30 July 2018. DOI: 10.1139/cjfr-2018-0006.
http://www.nrcresearchpress.com/toc/cjfr/0/ja

969 The brightness was calculated as the average of the tree channel. Next, the brightness layer
970 was filtered using a 3 by 3 kernel with 1/9 cell value. Finally, all pixels along a line were
971 extracted. The line started near the optical axis and ended at the border of the image,
972 passing over the white paper strip. The script is available from the first author upon request.
973 Figure 1 shows that changing the aperture did not modify the vignetting effect. Similar results
974 were reported by Lang et al. (2010) for the Nikon FC-E8 converter attached to the Nikon
975 Coolpix 4500.
976

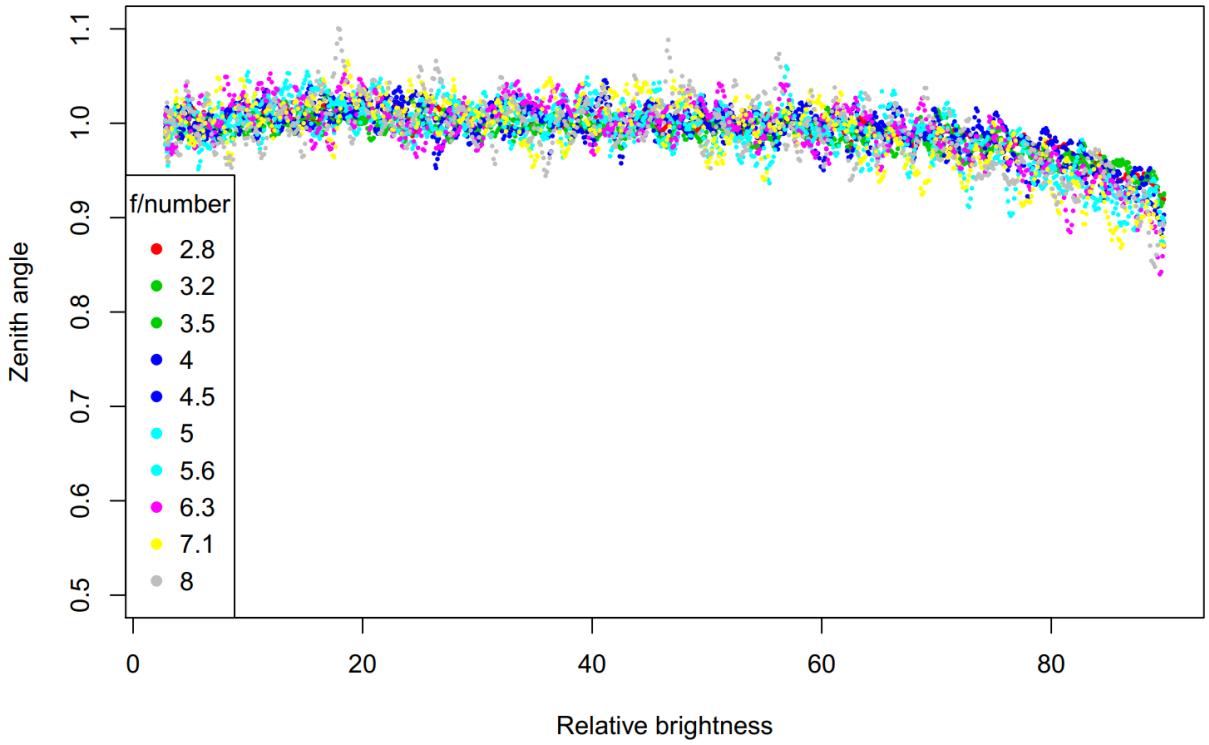

977

978 Figure 1. Measured vignetting for the Nikon FC-E9 converter attached to the Nikon Coolpix
979 5700 camera. The relative brightness of a target with uniform radiance appears to decrease
980 when the zenith angle increases. The points were extracted from photographs taken with the
981 ten different f-numbers that the camera supports. The points form a compact cloud with a
982 clear tendency, showing that the aperture did not modify the vignetting effect.
983

Author version of the manuscript published for Canadian Journal of Forest Research on the web 30 July 2018. DOI: 10.1139/cjfr-2018-0006.
http://www.nrcresearchpress.com/toc/cjfr/0/ja

References

Wagner, S. 2001. Relative radiance measurements and zenith angle dependent segmentation in hemispherical photography. Agric. For. Meteorol. **107**(2): 103–115. doi:10.1016/S0168-1923(00)00232-X.

Lang, M., Kuusk, A., Mõttus, M., Rautiainen, M., and Nilson, T. 2010. Canopy gap fraction estimation from digital hemispherical images using sky radiance models and a linear conversion method. Agric. For. Meteorol. **150**(1): 20–29. doi:10.1016/j.agrformet.2009.08.001.

S5

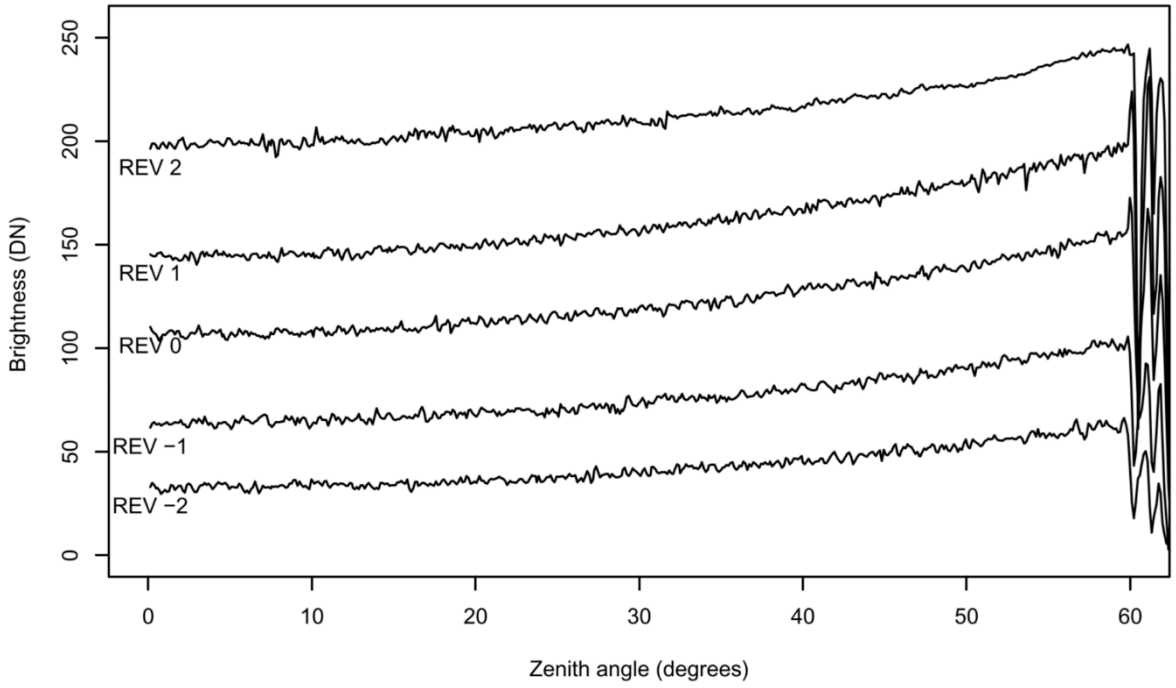

Figure 1. Sky profile extracted from a series of photographs taken in summer at 19:45 hours. The sky was free of obstacles up to approximately 57 degrees. Brightness is the average of the three channels.